Hindawi
International Journal of Energy Research
Volume 2023, Article ID 4938451, 23 pages
https://doi.org/10.1155/2023/4938451

WILEY | Hindawi

Research Article

Fuzzy Airflow-Based Active Structural Control of Integrated Oscillating Water Columns for the Enhancement of Floating Offshore Wind Turbine Stabilization

Fares M'zoughi,[1] **Izaskun Garrido**,[1] **Aitor J. Garrido**,[1] **and Manuel De La Sen**[2]

[1]*Automatic Control Group (ACG), Institute of Research and Development of Processes (IIDP), Department of Automatic Control and Systems Engineering, Faculty of Engineering of Bilbao, University of the Basque Country (UPV/EHU), Po Rafael Moreno No. 3, 48013 Bilbao, Spain*
[2]*Automatic Control Group (ACG), Institute of Research and Development of Processes (IIDP), Department of Electricity and Electronics, Faculty of Science and Technology, University of the Basque Country (UPV/EHU), Bo Sarriena s/n, 48080 Leioa, Spain*

Correspondence should be addressed to Fares M'zoughi; fares.mzoughi@ehu.eus

Received 7 October 2022; Revised 3 January 2023; Accepted 12 January 2023; Published 7 February 2023

Academic Editor: Keat Teong Lee

This paper presents the modeling and stabilization of a floating offshore wind turbine (FOWT) using oscillating water columns (OWCs) as active structural control. The novel concept of this work is to design a new FOWT platform using the ITI Energy barge with incorporated OWCs at opposite sides of the tower, in order to alleviate the unwanted system oscillations. The OWCs provide the necessary opposing forces to the bending moment of the wind upon the tower and the waves upon the floating barge platform. However, the forces have to be synchronized with the tilting of the system which will be ensured by the proposed fuzzy airflow control strategy. Using the platform pitch angle, the fuzzy airflow control opens the valve of one side and closes the valve of the other side accordingly. Results of simulation in comparison with the standard FOWT and a PID-based airflow control show the efficiency of the fuzzy airflow control and its superiority to decrease the platform pitching and the top tower fore-aft displacement.

1. Introduction

The expansion of industries and growing population has increased the demand for energy [1]. To meet these demands in the energy market, research and development is now pushing toward the exploitation of renewable energy [2]. One of the leading commercial renewable energy resources is wind energy with a substantial potential in the area of onshore and offshore [3, 4]. Therefore, wind energy has been widely promoted in the energy source composition [5]. Consequently, a fast growth in global wind energy production has been registered during the last decade [6]. In fact, the overall installed capacity for onshore wind turbines (WTs) has increased to 651 GW in 2019 from 159 GW in 2009. Particularly, a high growth in the annual installed offshore WT capacity has been recorded in 2019. On the other hand, the production of offshore wind energy has been noticeably accelerating and becoming a significant key aspect of the global wind energy industry roadmap [7]. The overall installed capacity for offshore WTs has improved to 29 GW in 2019 from 2 GW in 2009 [6]. The new estimated annual offshore installed capacity has been approximated to surpass 30 GW by 2030, with a combined yearly increase of 18.6% and 8.2% during the first half and second half of the decade [3].

With the accelerating of offshore wind energy production, coastal space limitations, and higher wind speed quality off the shores, floating offshore wind turbines (FOWTs) emerge as a promising alternative to the onshore wind turbines the future. In this context, nowadays, many efforts

have been invested towards FOWTs thanks to their promising potential to contribute to global energy production and its environmentally friendly features [8, 9]. In fact, the offshore wind market recorded a growth of 6.1 GW in 2020 compared to from 2.2 GW in 2016, raising the share of new offshore wind installations from 4% to 7% [10]. This growth may be traced to the stable progress in Europe representing the majority of the remaining new capacity, led by the Netherlands which managed to install by the year 2020 around 1.5 GW of new offshore wind, second by Belgium, which managed to install 706 MW [10]. Even though presented offshore wind capacity turned out fairly less during 2020 in comparison to 2019, over 7 GW of offshore wind auctions or tenders was initiated. Out of these auctions, 5.5 GW is via solicitations issued by the states of New Jersey, New York, and Rhode Island in the USA. The remaining capacities can be traced to Denmark (800-1000 MW) and Japan [10].

Many offshore wind platforms have been proposed and developed to achieve static stability. Four main foundations emerged with different concepts. The first concept is the spar buoy, which consists of a ballast stabilized with catenary mooring drag embedded anchors [11]. SPAR is a vertical cylinder using heavy ballast at the lower extremity to provide stability and shifting the center of gravity underneath the center of buoyancy. The world's first commercial wind farm which uses FOWTs was Hywind Scotland in 2017. It is located 29 km from the shores of Peterhead, Scotland. The wind farm holds a total of five 6 MW Hywind SPAR turbines accumulating a combine capacity of 30 MW [12]. The second concept is the tension leg platform (TLP), which is a mooring line stabilized TLP with suction pile anchors [13]. For this concept, the structure's stability is ensured by using multiple taut mooring lines rather than stabilizing it using the buoyancy obtained from the underwater geometry [14]. The world's first FOWT using a TLP was deployed by Blue H Technologies of the Netherlands. This floating platform has been deployed in Italy, 21.3 km off the shores of Apulia in December 2007 [15]. The third concept is the semisubmersible type, which consists of a buoyancy stabilized with catenary mooring lines. This type of platform consists of columns that constitute the core volume below the seawater and rigid joining parts that ensures structural integrity of the entire structure [16]. The first adopter of the semisubmersible in FOWTs was WindFloat. The WindFoat technology binds three columns using braces, and the WT is mounted upon one of the three columns [17]. DeepCwind technology uses three columns and a fourth one in the center to support the WT [18]. The fourth concept is the barge platform, which is considered by many as a subtype of semisubmersible concept. It is a buoyancy stabilized with catenary mooring lines but with large waterplane area [19]. FLOATGEN is the first offshore wind turbine in France and BW Ideol's first demonstrator using a barge type platform with a 2 MW capacity installed 20 km off the shores of Le Croisic on the offshore experimentation site SEM-REV of the Ecole Centrale de Nantes [20]. Recently, Chuang et al. in [21] studied the stability and the mooring system reliability of this type of FOWT platform by using a 1 : 64 scaled model. The results showed that the wave frequency motion mainly induced the motion in a vertical plane (e.g., heave, roll, and pitch), whereas the low-frequency slow drift motion mainly caused the motion in the horizontal plane (e.g., surge, sway, and yaw). The mooring system showed a significant role to repel low-frequency motions, particularly in shallow waters.

The development and deployment of FOWT systems raised attention to some issues. These issues are related to structural behavior caused by loads induced by wind upon the tower and the wave upon the platform [22]. These loads increase stress, failures, possibility of damages, and maintenance expenses whereas reducing its efficiency and lifetime. Several concepts were introduced to alleviate the loads, which may be categorized to two approaches. The first approach consists of using the rotor thrust as a restoring torque to decrease FOWT pitching which may be done through the adjustment of the blades' pitch angle. Jonkman and Jonkman and Matha performed numerous investigation and developed the software FAST (Fatigue, Aerodynamics, Structures, and Turbulence) and designed a baseline collective-pitch control for blade pitch for three major FOWTs by means of a gain scheduled proportional-integral strategy [23, 24]. Lackner regulated, in [25], the pitch angle of the blade through varying the rated rotor velocity. Varying the rotor velocity directly induces the generation of additional restoring torque. Staino and Basu used, in [26], a dual control joining passive pitch control and the active tendons within the blades' empty body to ease aerodynamic loads upon the blades. Recently, Yang et al. proposed in [27] a new concept combing the assets of a spar-type platform and semisubmersible platform. A study conducted by Cheung et al. in [28] of barge platform consisting of an array of connected vertical cylinders which are open at the bottom to trap pressurized air showed that properly tuning the pneumatic platform may be an interesting design idea for big floaters or wave energy converters (WEC). The second method for load mitigation is by means of structural controls. Lackner created FAST-Structural Control (FAST-SC), which is a modified version of the software FAST and is a high fidelity simulation software that takes into consideration structural control in FOWTs by means of a passive tuned mass damper (TMD) mounted within the nacelle using Kane's dynamics. Lackner used FAST-SC in [25] for a TMD installed within the nacelle. Thus, 2 degrees of freedom (DoF) of the TMD were introduced to the kinetic equations. Lackner and Rotea optimized, in [29], the TMD for a barge-based FOWTs using FAST-SC. Luo et al. in [30] assumed that the FOWT is a lump-like mass and employed a tuned liquid column damper (TLCD) to reduce the surge displacement. Hu and He created, in [31], an active structural control using a stroke-limited hybrid mass damper employing linear-quadratic regulator. A quantitative study has been performed by Jonkman and Matha in [24] between the three types of floating platforms (i.e. Spar, TLP, and barge) with respect to the technological challenges. This study investigates the quantitative analysis of a NREL 5 MW system mounted on the MIT/NREL TLP, the OC3-Hywind spar buoy, and the ITI Energy barge and using a

detuned baseline collective blade-pitch controller. Results of the dynamic responses showed that the platform motion-induced ultimate and fatigue loads for all turbine components in the ITI Energy barge are the highest loads. In addition, the differences in the ultimate and fatigue loads between the MIT/NREL TLP system and the OC3-Hywind system are not significant, except for the loads in the tower, which are greater in the OC3-Hywind system. However, the results are purely quantitative and not qualitative without further considerations (especially economic); hence, no definite statement could be made about which concept or hybrid thereof is likely the "best."

Other ideas proposed the development of multipurpose platform, which combines different renewable energy. This way companies make better use of the expensive platform by extracting more energy from multiple sources at once, efficiency, and cost reduction. Wind-wave energy platforms are the most reputed combination and most suitable ones for deep offshore waters [32–35]. The use of the WEC with a FOWT has been suggested and showed encouraging outcomes. Kluger et al. [36] studied the usage of wave energy converter array with a spar-based FOWT known as OC3-Hywind. Ma et al. studied in [37] the effect of the typhoon on OC3-Hywind's aerodynamic performance. Slocum et al. [38] investigated the effects of using an outer and inner heaving wave energy converters with the same floating system. Kamarlouei et al. [39] established that wave energy converter array implementation can reduce the system's oscillations in heave and pitch modes. Recently, Khatibani and Ketabdari studied in [40] the dynamics and power absorption of a proposed hybrid monopile WT and two pitching wave energy converters. Nevertheless, the presented methods have not implemented OWCs in FOWTs using barge platforms.

With the suggestion of hybrid floating wind platforms, the need to advanced control strategies had a significant effect on the successful implementation of many concepts. For instance, in [31], Hu and He designed a state-feedback linear quadratic regulator (LQR) controller to reduce vibration and loads of the wind turbine. Zhu and Changhong developed in [41] a hybrid model predictive control (HMPC) to control the power take-off (PTO) of wave energy converters combined with a floating semisubmersible platform. However, the weighting parameters Q and R in the performance index have a great influence on the control effect, and inappropriate weighting coefficients can lead to the control failure. Sierra-García and Santos used in [42] the neural networks and reinforcement learning to control the blade pitch angle. Li and Huijun in [43] implemented a H_∞ controller for a TMD installed at the barge platform instead of the nacelle. However, the H_∞ needs so much active TMD power that it may not be an economical design; also, the H_∞ structural controller has the reliability issue in dealing with a wind turbine fault. In [44], Yang et al. developed an individual blade control using a fuzzy logic controller (FLC) along with an MPC module and a disturbance estimator module. The FLC module is what combines all three parts while ensuring smooth transitions. The simplicity of the FLC design, the unruffled operation, and the cheap cost of implementation demonstrate it as a promising control choice for this research work.

This work proposes the combination of a FOWT with OWCs to harvest wave and wind power and to investigate the stabilization of the floating platform of the 5 MW FOWT by means of the integrated OWCs [45, 46]. The studied floating system is the NREL 5 MW wind turbine fixed on top of a barge platform. The concept is aimed at incorporating OWCs into a barge to decrease the unwanted oscillations of the system [46]. The stabilization can be accomplished with the control of the air valves of each OWC using an airflow control approach [47–49]. This allows the adjustment of airflow and pressure in the air chambers. In this paper, a fuzzy airflow control has been suggested and implemented to effectively open or close the air valves of the incorporated OWCs collectively. The performance of the suggested fuzzy airflow control has been compared to a PID-based airflow control [45] and the standard barge FOWT.

The remainder of the paper is arranged to the following sections: Section 2 details the equations of the proposed model of the hybrid OWC and floating offshore wind turbine mathematical description. Section 3 introduces the fuzzy airflow control designed to regulate the airflow and pressure within the OWC air chamber to stabilize the system. A study comparing the FOWT's structural behavior among the standard barge, the PID-controlled OWC-based barge, and the fuzzy-controlled OWC-FOWT is interpreted in Section 4. Lastly, Section 5 finishes the article with several concluding observations.

2. Proposed Hybrid Wind-Wave Floating Offshore Wind Turbine

The study performed in this research work investigates the stabilization of the FOWT shown in Figure 1.

In this paper, the system studied is the NREL 5 MW baseline WT fixed on an ITI Energy barge. The ITI Energy barge is a concept that was developed by Vijfhuizen at the Department of Naval Architecture and Marine Engineering at the Universities of Glasgow and Strathclyde through a contract with ITI Energy (please see [50] for further details).

This type of platform is a square platform, which has been frequently investigated for load analysis and conception verification of FOWTs. It has been specifically designed for the purpose of harvesting wind and wave energy [50].

The WT under study is upwind type, has three blades, and uses variable speed and collective pitch controls. A generator, located in the nacelle at the top of the tower with an altitude of 90 m, is driven by these blades. The WT is fixed on top of a ballasted barge platform. The ITI Energy barge under study is a square and is ballasted with seawater to achieve a reasonable draft, which is not so shallow that it is susceptible to incessant wave slamming. To prevent it from drifting, the platform is moored by a system of eight slack, catenary lines. Two of these lines emanate from each corner of the bottom of the barge such that they are 45° apart at the corner. This type of platform has been specifically designed for the purpose of harvesting wind and wave energy. Therefore, its shape and size are accommodating for WEC incorporation. Moreover, its resulting natural frequency has proven to be a key factor to the improvement of

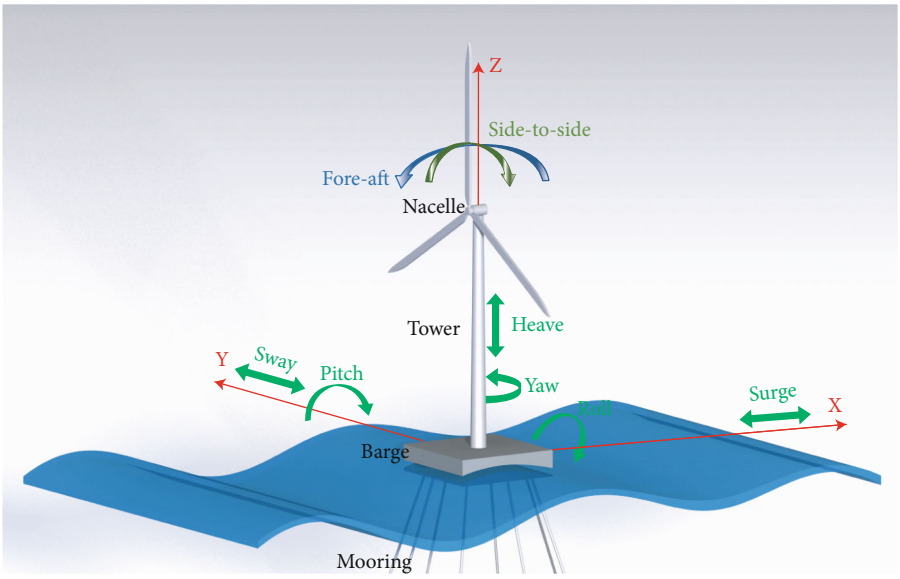

Figure 1: Scheme of floating offshore wind turbine.

structural behavior of wave-wind floating platforms [19, 46]. In this sense, it has been frequently investigated for load analysis and conception verification of FOWTs [24].

Parameters of the 5 MW WT and the ITI Energy barge are detailed in [23], from which the most relevant features are listed in Table 1.

In this work, the study will focus on the vibration reduction in the proposed hybrid wind-wave floating offshore wind turbine system with heading wave along the x-axis while using the developed fuzzy airflow control. In this sense, the study will focus on the varying DOFs along the x-axis (i.e., surge, pitch, and fore-aft). Even though the barge platforms have big surge displacement, studies showed that the platform pitch has the highest effect on the tower bending [51]. Therefore, only the pitch mode has been enabled while the surge mode has been disabled. This method has been proven to be sufficiently efficient for structural vibration control of FOWTs [29, 31, 52]. For that reason, the developed model of the proposed hybrid plant emphasizes on two motions, namely, the barge platform's pitch angle and the top tower's fore-aft displacement.

2.1. Dynamic Model of the Hybrid Wind-Wave Floating Offshore System. In barge-based FOWTs, the most contributing DOFs to the bending moments of the tower are the pitch angle of the barge platform and the fore-aft displacement of the tower [53–55]. Hence, these two DOFs have been taken into consideration to design a simplified reduced-order model of the proposed combined wind-wave floating platform. The mathematical model adopted from [31, 52] uses Euler-Lagrange's equations and is widely used for this type of problem. The scheme of the suggested hybrid floating platform is illustrated in Figure 2.

The WT tower is presumably linked to the barge platform using torsional spring and damper acting as the structural stiffness k_t and damping d_t. The stiffness of the mooring system and hydrostatic restoring torques acting on the platform is modeled using a spring constant k_p, and the hydrodynamic damping, including viscous and radiation effects of the waves, is represented using a damping coefficient d_p.

The concept of integrating two OWCs within the barge platform is to help mitigate the platform's pitch angle and tower fore-aft displacement. In this research, the focus has been to reduce oscillations around the y-axis; therefore, two identical OWCs have been considered and integrated in front and at the back of the tower at equal distance to preserve symmetry along the x-axis as illustrated in Figure 2.

For a nonconservative system consisting of n generalized degrees of freedom, Euler-Lagrange's expression is defined as

$$\frac{d}{dt}\left(\frac{\partial L}{\partial \dot{q}_i}\right) - \frac{\partial L}{\partial q_i} = Q_i, \tag{1}$$

$$L = T - V, \tag{2}$$

where T represents the total kinetic energy, V represents the total potential energy, L stands for the Lagrange operator, and Q_i represents the generalized nonpotential forces.

The total kinetic and potential energies of the studied FOWT may be described as

$$T = \frac{1}{2} I_t \dot{\theta}_t^2 + \frac{1}{2} I_p \dot{\theta}_p^2, \tag{3}$$

$$V = \frac{1}{2} k_t \left(\theta_t - \theta_p\right)^2 + \frac{1}{2} k_p \theta_p^2 + m_t g R_t \cos\theta_t - m_p g R_p \cos\theta_p, \tag{4}$$

where R_p and R_t are the distances measured from the mass centers (MCs) until the tower hinge.

Table 1: Parameters of the NREL 5 MW wind turbine and the ITI Energy barge.

Wind turbine		ITI Energy barge	
Feature	Value	Feature	Value
Rating power	5 MW	Platform size	40 m × 40 m × 10 m
Baseline control	Variable speed, collective pitch	Platform mass	5,452,000 kg
Cut-in, rated, cut-out wind speed	3 m/s, 11.4 m/s, 25 m/s	Anchor depth	150 m
Cut-in, rated rotor speed	6.9 rpm, 12.1 rpm	Number of mooring lines	8
Tower mass	347,460 kg	Line diameter	0.0809 m
Rotor diameter	126 m	Line mass density	130.4 kg/m
Hub height	90 m		

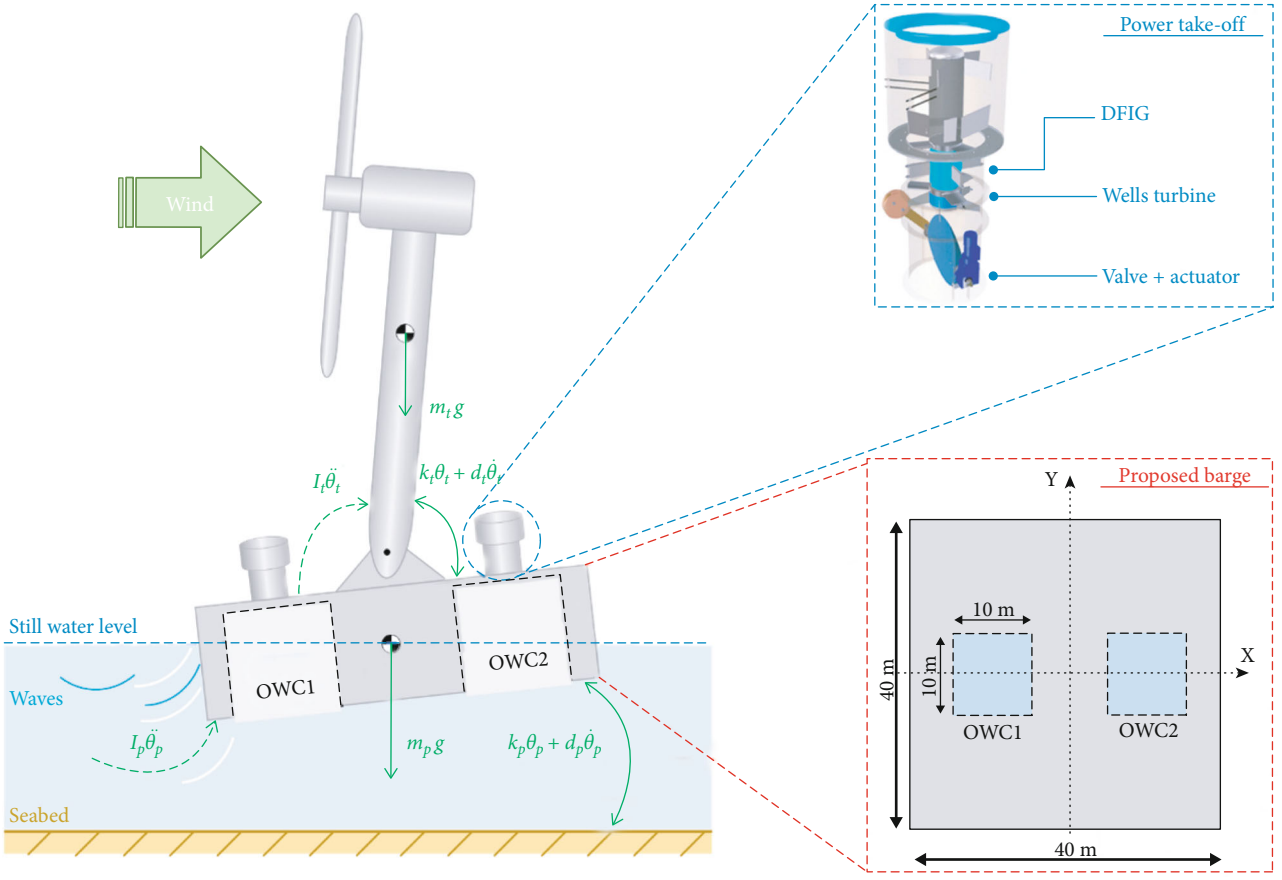

Figure 2: Scheme of the proposed hybrid wind-wave floating system.

The generalized nonpotential forces include the forces excited by winds and waves as

$$\begin{cases} Q_{\theta_t} = -d_t\left(\dot{\theta}_t - \dot{\theta}_p\right) + M_{\text{wind}}, \\ Q_{\theta_p} = -d_p\dot{\theta}_p + d_t\left(\dot{\theta}_t - \dot{\theta}_p\right) + M_{\text{wave}} - R_{\text{OWC1}}f_{\text{OWC1}} + R_{\text{OWC2}}f_{\text{OWC2}}, \end{cases} \tag{5}$$

where θ is the rotation angle from the vertical z-axis and k and d represent the spring stiffness and damping coefficients. m represents the mass, and I represents the inertia moment from the MCs. R_{OWC1} and R_{OWC2} are the distances measured from MCs of the OWCs until the tower hinge. M_{wind} and M_{wave} are the bending torques induced by wind and wave loads, respectively. f_{OWC1} and f_{OWC2} are the forces produced by the pressure in the OWC air chambers.

Small angle approximations were used due to the fact that the pitch angle of FOWT structures does not exceed 10 degrees, even during the roughest winds and waves [31, 52] and also considering that the OWC1 and OWC2 are equidistant to the tower base (R_{OWC1}=R_{OWC2}=R_{OWC}). As a

result, by substituting (3), (4), and (5) into (1) and (2), the dynamic model may be defined as

$$\begin{cases} I_p\ddot{\theta}_p - k_t\left(\theta_t - \theta_p\right) + k_p\theta_p + m_p g R_p\theta_p = -d_p\dot{\theta}_p + d_t\left(\dot{\theta}_t - \dot{\theta}_p\right) + M_{\text{wave}} - R_{\text{OWC}}(f_{\text{OWC1}} - f_{\text{OWC2}}), \\ I_t\ddot{\theta}_t + k_t\left(\theta_t - \theta_p\right) - m_t g R_t\theta_t = -d_t\left(\dot{\theta}_t - \dot{\theta}_p\right) + M_{\text{wind}}. \end{cases} \tag{6}$$

Let the M, D, and K be the inertia, damping, and stiffness matrices, respectively:

$$\begin{aligned} X &= \begin{bmatrix} \theta_p \\ \theta_t \end{bmatrix}, \\ M &= \begin{bmatrix} I_p & 0 \\ 0 & I_t \end{bmatrix}, \\ D &= \begin{bmatrix} d_p + d_t & -d_t \\ -d_t & d_t \end{bmatrix}, \\ K &= \begin{bmatrix} k_p + k_t + m_p g R_p & -k_t \\ -k_t & k_t - m_t g R_t \end{bmatrix}. \end{aligned} \tag{7}$$

Thus, the system's equations of (6) can be rewritten as

$$M\ddot{X} + D\dot{X} + KX = EM_{\text{ext}} + RF, \tag{8}$$

where

$$\begin{aligned} M_{\text{ext}} &= \begin{bmatrix} M_{\text{wind}} \\ M_{\text{wave}} \end{bmatrix}, \\ R &= \begin{bmatrix} -R_{\text{OWC}} & 0 \\ 0 & 0 \end{bmatrix}, \\ E &= \begin{bmatrix} 0 & 1 \\ 1 & 0 \end{bmatrix}, \\ F &= \begin{bmatrix} f_{\text{OWC1}} - f_{\text{OWC2}} \\ 0 \end{bmatrix}. \end{aligned} \tag{9}$$

Equation (8) can be further arrange to a state-space model as follows:

$$\dot{X}_m = A_m X_m + B_m F + B_{\text{ext}} M_{\text{ext}}, \tag{10}$$

where

$$\begin{aligned} X_m &= \begin{bmatrix} X \\ \dot{X} \end{bmatrix}, \\ A_m &= \begin{bmatrix} 0 & I \\ -M^{-1}K & -M^{-1}D \end{bmatrix}, \\ B_m &= \begin{bmatrix} 0 \\ M^{-1}R \end{bmatrix}, \\ B_{\text{ext}} &= \begin{bmatrix} 0 \\ M^{-1}E \end{bmatrix} \end{aligned} \tag{11}$$

Winds and waves interact with the floating system in a complex aeroelastic and hydroelastic manner. Furthermore, wind- and wave-induced structural responses possess inherent connection [56]. For linear modeling, the wind and wave loads M_{wind} and M_{wave} were presumed to be linearly attained wind speed $V_{\text{wind}}(t)$ and the wave height $Z(t)$; therefore, M_{wind} and M_{wave} have been modeled as first-order functions [56]:

$$\dot{M}_{\text{wind}}(t) = -\alpha_{\text{wind}} M_{\text{wind}} + \beta_{\text{wind}}\, V_{\text{wind}}(t), \tag{12}$$

$$\dot{M}_{\text{wave}}(t) = -\alpha_{\text{wave}} M_{\text{wave}} + \beta_{\text{wave}}\, Z(t). \tag{13}$$

Using equations (12) and (13) in equation (10), the described system can be written as

$$\dot{X} = AX + BU + B_w W, \tag{14}$$

where

$$X = \begin{bmatrix} X_m \\ M_{\text{wind}} \\ M_{\text{wave}} \end{bmatrix},$$
$$A = \begin{bmatrix} A_m & B_{\text{ext}} \\ 0 & \alpha \end{bmatrix},$$
$$B = \begin{bmatrix} B_m \\ 0 \end{bmatrix},$$
$$B_w = \begin{bmatrix} 0 \\ \beta \end{bmatrix},$$
$$U = \begin{bmatrix} F \\ 0 \end{bmatrix}, \quad (15)$$
$$W = \begin{bmatrix} V_{\text{wind}}(t) \\ Z(t) \end{bmatrix},$$
$$\alpha = \begin{bmatrix} \alpha_{\text{wind}} & 0 \\ 0 & \alpha_{\text{wave}} \end{bmatrix},$$
$$\beta = \begin{bmatrix} \beta_{\text{wind}} & 0 \\ 0 & \beta_{\text{wave}} \end{bmatrix}.$$

In conclusion, the platform pitch angle θ_p and the top tower displacement of fore-aft (TTD_{FA}) are attained:

$$Y = CX, \quad (16)$$

where

$$C = \begin{bmatrix} 1 & 0 & 0 & 0 & 0 & 0 \\ -H_T & -H_T & 0 & 0 & 0 & 0 \end{bmatrix} \quad (17)$$

with H_T is the hub height and

$$Y = \begin{bmatrix} \theta_p \\ TTD_{FA} \end{bmatrix}. \quad (18)$$

In the case where other wave directions are considered instead of the heading waves, two more DOFs will be included, namely, the platform roll angle and the tower top side-to-side displacement. Also, two OWCs will be integrated at the sides (left and right) to deal with the vibrations affecting the roll and side-to-side DOFs.

Lastly, the structural parameters of the NREL 5 MW wind turbine and the ITI Energy barge platform are adopted from [31] by Hu and He (see Table 2). The parameters have been obtained by identification process after defining the mathematical FOWT model using the modified FAST-SC software. The FAST-based FOWT model had been used as a baseline tool to make a simulation, and the results are compared with the results made by the proposed Euler-Lagrange mathematical model as detailed in [31, 57].

2.2. Oscillating Water Columns Opposing Forces. Since ocean waves are larger than nearshore waves, it is possible to assume that waves are large enough to consider the oscillating water free-surface inside the OWC chambers as one rigid body heaving inside the column along the vertical axis. Hence, it is possible to assume that the internal free surface inside the OWC's chamber behaves like a piston and the pressure is uniform according to the following assumptions:

(i) The ocean waves are large enough to make the water free-surface inside the chambers oscillate as the same body (piston)

(ii) The water free-surface inside the capture chambers only oscillates along the chamber's vertical axis

(iii) The water free-surface is a rigid piston with a thickness that may be nonzero, but the sum of the mass and added mass of the rigid piston is practically independent of its thickness

Assume that the water free surface in the capture chamber acts similar to a piston which allows us to consider the pressure uniform. Hence, the oscillating forces can be described by [55]

$$f_{\text{OWC}i} = -p_i(t)\, S, \quad (19)$$

where $p_i(t)$ and S are the pressures in the chamber and inner free surface, $i = 1, 2$ referring to OWC1 or OWC2.

Considering the air inside the capture chamber to be an ideal gas and the chamber is adiabatic and the transformations are adequately slow to be considered reversible, consequently, the transformations can be assumed isentropic and the expression of the air density can be written as

$$\rho_i(t) = \rho_a \left(\frac{p_i(t)}{p_a} \right)^{1/\gamma}, \quad (20)$$

where p_a and ρ_a stand for atmospheric pressure and density and γ represents the air-specific heat ratio.

The former isentropic expression may be linearized to get:

$$\rho_i(t) = \rho_a \left(\frac{p_i(t)}{p_a \gamma} \right), \quad (21)$$

$$\dot{\rho}_i(t) = \frac{\rho_a}{p_a \gamma} \dot{p}_i(t). \quad (22)$$

Table 2: Structural features of the NREL 5 MW wind turbine and the ITI Energy barge platform.

Tower		Barge platform	
Feature	Value	Feature	Value
Stiffness	$k_t = 9.7990\ 10^9$ (N m rad^{-1})	Stiffness	$k_p = 1.4171\ 10^9$ (N m rad^{-1})
Damping coefficient	$d_t = 2.1032\ 10^7$ (N m s rad^{-1})	Damping coefficient	$d_p = 3.6374\ 10^7$ (N m s rad^{-1})
Inertia	$I_t = 1.8217\ 10^9$ (kg m^2)	Inertia	$I_p = 1.6945\ 10^9$ (kg m^2)

Using the linearized forms of (21) and (22), the mass flow rate of the air within chambers can be defined by

$$\dot{m}_i(t) = \frac{d}{dt}\left(\rho_i(t)\, V_{\mathrm{OWC}i}(t)\right) = \frac{\rho_a V_0}{p_a \gamma}\dot{p}_i(t) + \rho_a\, \dot{V}_{\mathrm{OWC}i}(t), \tag{23}$$

where V_0 and $V_{\mathrm{OWC}}(t)$ are the chamber's undisturbed and the instantaneous air volumes.

The air volume is dependent on the chamber's shape and thus may be defined as

$$V_{\mathrm{OWC}i}(t) = V_0 - S\, Z_i(t), \tag{24}$$

where $S = lc.wc$ is the chamber's inner free surface and Z_i is the vertical displacement of the air, rising in the ascending direction.

The vertical displacement of the air in the chamber is defined as the difference between the heaving body of the chamber Z_P and the oscillating piston-like water surface Z_{Wi} as

$$Z_i(t) = \left(Z_P(t) - Z_{Wi}(t)\right), i = \{1, 2\}, \tag{25}$$

where Z_{Wi} is the displacement of the oscillating piston-like water surface in each of the two OWC chambers.

The displacement of the piston-like water surface Z_{Wi} is obtained based on the type of wave elevation function, which in this work is the regular wave. Hence, Z_{Wi} is described as

$$Z_{Wi}(x_i, t) = \frac{H}{2}\cos\left(k\, x_i - \omega t\right), i = \{1, 2\}, \tag{26}$$

where x_i will be considered as the center of mass of the piston-like water in each chamber, k is the wave number, and H is the wave height.

Therefore, the pressure inside the chamber varies with the mass flow rate and the air volume:

$$\dot{p}_i(t) = \frac{p_a \gamma}{\rho_a V_0}\dot{m}_i(t) - \frac{p_a \gamma}{V_0}\dot{V}_i(t). \tag{27}$$

Considering that the OWCs are equipped with Wells turbines, hence its turbomachinery formulas are taken into consideration. Therefore, the dimensionless flow coefficient may be expressed as

$$\Phi = \frac{\dot{m}}{\rho_a \omega r^3}, \tag{28}$$

where r and ω are the radius and rotational velocity. The flow coefficient of a Wells turbine may be defined using the air axial speed as

$$\Phi = \frac{v_x}{r\omega}, \tag{29}$$

where v_x is the air axial speed crossing the turbine.

The volume flow rate can be defined by the axial velocity as

$$Q = \frac{dV}{dt} = a v_x, \tag{30}$$

where a is the cross-sectional surface of the Wells turbine.

By replacing (28)–(30) in (27), the pressure is obtained against the airflow velocity as

$$\dot{p}_i(t) = \frac{p_a \gamma}{V_0} r^2 v_{xi}(t) - \frac{p_a \gamma}{V_0} a v_{xi}(t). \tag{31}$$

The parameters of the Wells turbine and the capture chamber constituting both OWCs are listed in Table 3.

3. Fuzzy Airflow-Based Active Structural Control

The integrations of the OWCs are intended to create forces prompted from the pressures enclosed inside the air chambers. These forces will resist some of the hydrodynamic forces. Since the OWCs were incorporated into the barge platform at opposite side of the tower, hence they will have opposing moments. In both OWCs, one air valve is installed at the top of the capture chamber which opens and closes the mouth of the air duct leading up to the Wells turbine. When the water oscillates from the bottom of the capture chamber, the air will flow upward and downward through the duct at the top. The opening and closing of the air valve will compress or decompress the air inside the chamber. To trap the air inside the chambers during wave crest and create pressure, the air valves have to be closed whereas to release air and decompress the air in the chamber during wave through the air valve should be opened. Seeing that the wave crest and wave through progressively passes the barge platform, each valve should be opened and closed gradually.

Table 3: Parameters of the considered OWCs.

Capture chamber		Wells turbine	
Feature	Value	Feature	Value
Chamber's inner width	$w_c = 10\,\text{m}$	Blade number	$n = 5$
Chamber's inner length	$l_c = 10\,\text{m}$	Blade span	$b = 0.21\,\text{m}$
Chamber's inner height	$h_c = 9\,\text{m}$	Blade chord length	$l = 0.165\,\text{m}$
Water density	$\rho_w = 1029\,\text{kg/m}^3$	Turbine mean radius	$r = 0.375\,\text{m}$
Atmospheric density	$\rho_a = 1.19\,\text{kg/m}^3$	Cross-sectional area	$a = 0.4417\,\text{m}^2$
Atmospheric pressure	$p_a = 101.325\,\text{kPa}$		

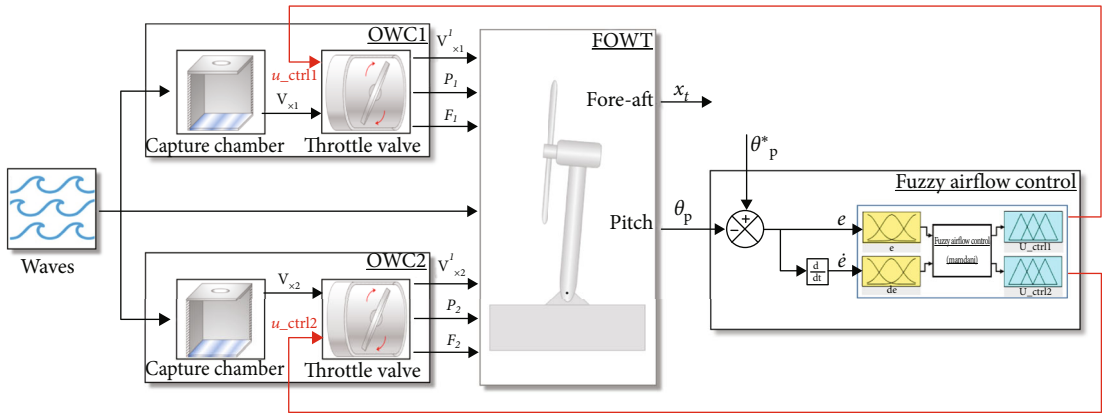

Figure 3: Block diagram of the suggested fuzzy airflow control for the OWC-FOWT stabilization.

Therefore, this paper proposes a fuzzy airflow control to adequately control the valves.

The suggested fuzzy airflow control depends on the platform pitch angle θ_p as shown in Figure 3. The input to the OWC-FOWT model is the wave height $Z(t)$ that may be obtained by using a wave height sensor fixed at the center of the barge or by using an acoustic Doppler current profiler fixed underneath the platform. The outputs of the developed model are the platform pitch angle θ_p and tower top fore-aft displacement x_t, which can be obtained using two accelerometers located at the top and bottom of the tower [55].

The suggested airflow control employs a fuzzy logic controller (FLC) to ensure the opening and closing of the air valves adequately based on the pitch angle as explained by Figure 3. The inputs of the fuzzy controller are the platform pitch angle error and its derivatives e and de, and the outputs are the control signals of the air valves U_{ctrl1} and U_{ctrl2}. As the waves oscillate, the opening and closing of the valves release or trap the air leading to compression or decompression of the air in the chambers p_1 and p_2. Subsequently, forces in the chambers, f_{OWC1} and f_{OWC2}, are created to oppose to the hydrodynamic forces imposed upon the barge platform.

The fuzzy inference system of the designed FLC possesses two inputs and two outputs as explained in Figure 3. The crisp outputs U_{ctrl1} and U_{ctrl2} are supposedly be in the predefined intervals $[U_{\text{ctrl1}}^{\min}, U_{\text{ctrl1}}^{\max}]$ and $[U_{\text{ctrl2}}^{\min}, U_{\text{ctrl2}}^{\max}]$. These intervals were defined based on the actuators of the throttle valve in both OWC1 and OWC2.

The fuzzy output signals for the valves of OWC1 and OWC2 are obtained based on the commonly used normalization technique defined in [58] as

$$Y' = \frac{\left(Y - Y^{\min}\right)}{\left(Y^{\max} - Y^{\min}\right)}, \tag{32}$$

where Y is the crisp value of U_{ctrl1} and U_{ctrl2}, $Y^{\max}$ and $Y^{\min}$ are the max and min control values, and Y' is the fuzzy outputs U'_{ctrl1} and U'_{ctrl2} obtained using the fuzzy rules of the type IF-THEN as

$$\begin{aligned} &\text{IF } (e \text{ is } A_i \text{ and } de \text{ is } B_i), \\ &\text{THEN } \left(U'_{\text{ctrl1}} \text{ is } C_i \text{ and } U'_{\text{ctrl2}} \text{ is } D_i\right), \end{aligned} \tag{33}$$

where A_i, B_i, C_i, and D_i are the fuzzy sets and $i = 1, 2, m$.

3.1. Fuzzy Membership Function Design. The selection of the membership function (MF) shape is problem specific. Based on extensive review on many literatures, it can be concluded that the triangular MF is widely used because of its simplicity. Using various MF for given problems, usually Gaussian and triangular MFs are found to be closely performing well

and better than other types of MF [59, 60]. In specific, the triangular MF is found to be better than Gaussian MF. Sadollah [61] compared the response of the system with various MFs and conveyed that the triangular MF is superior to any other MFs.

When designing the triangular MFs of the FLC, based on the trial and error method, it is found that for input variables with small crisp values (i.e., e and de), it is better to change the left and/or right spread and/or overlapping towards zero to optimize the fuzzy controller performance. This type of spread is used instead of the straight symmetric triangular MFs with 50% overlap to optimize the controller performance [61].

The membership of the input e is obtained using the fuzzy sets A_i, which is defined by the functions illustrated in Figure 4.

Therefore, the mark of the membership functions μ_{A_i} of the input e is defined as

$$\mu_{A_i} = \begin{cases} \mu_{\mathrm{NB}}(e) = \begin{cases} 1 & \text{if } e \le -6, \\ \left(-\frac{e}{4} - \frac{1}{2}\right) & \text{if } e \in (-6,-2), \\ 0 & \text{if } e \ge -6, \end{cases} \\ \mu_{\mathrm{N}}(e) = \begin{cases} 0 & \text{if } e \le -6, \\ \left(\frac{e}{4} - \frac{3}{2}\right) & \text{if } e \in (-6,-2], \\ \left(-\frac{e}{2}\right) & \text{if } e \in (-2, 0), \\ 0 & \text{if } e \ge 0, \end{cases} \\ \mu_{\mathrm{Z}}(e) = \begin{cases} 0 & \text{if } e \le -2, \\ \left(\frac{e}{2} + 1\right) & \text{if } e \in (-2, 0], \\ \left(-\frac{e}{2} + 1\right) & \text{if } e \in (0, 2), \\ 0 & \text{if } e \ge 2, \end{cases} \\ \mu_{\mathrm{P}}(e) = \begin{cases} 0 & \text{if } e \le 0, \\ \left(\frac{e}{2}\right) & \text{if } e \in (0, 2], \\ \left(-\frac{e}{4} + \frac{3}{2}\right) & \text{if } e \in (2, 6), \\ 0 & \text{if } e \ge 6, \end{cases} \\ \mu_{\mathrm{PB}}(e) = \begin{cases} 0 & \text{if } e \le 0, \\ \left(\frac{e}{4} - \frac{1}{2}\right) & \text{if } e \in (2, 6), \\ 1 & \text{if } e \ge 6. \end{cases} \end{cases} \tag{34}$$

The membership functions defined for the input variables were of triangular and trapezoidal types. The linguistic levels used are the negative-big (NB), negative (N), zero (Z), positive (P), and positive-big (PB).

The membership degree of the input de is obtained using the fuzzy sets B_i, which is defined by the membership functions illustrated in Figure 5.

Therefore, the mark of the membership functions μ_{B_i} of the input de is defined as

$$\mu_{B_i} = \begin{cases} \mu_{\mathrm{NB}} = \begin{cases} 1 & \text{if } de \le -2, \\ \left(\frac{-2de}{5} - \frac{1}{5}\right) & \text{if } de \in \left(-2, \frac{-1}{2}\right), \\ 0 & \text{if } de \ge \frac{-1}{2}, \end{cases} \\ \mu_{\mathrm{N}} = \begin{cases} 0 & \text{if } de \le -2, \\ \left(\frac{2de}{5} - \frac{4}{5}\right) & \text{if } de \in \left(-2, \frac{-1}{2}\right], \\ (-2de) & \text{if } de \in \left(\frac{-1}{2}, 0\right), \\ 0 & \text{if } de \ge 0, \end{cases} \\ \mu_{\mathrm{Z}} = \begin{cases} 0 & \text{if } de \le \frac{-1}{2}, \\ (2de + 1) & \text{if } de \in \left(\frac{-1}{2}, 0\right], \\ (-2de + 1) & \text{if } de \in \left(0, \frac{1}{2}\right), \\ 0 & \text{if } de \ge \frac{1}{2}, \end{cases} \\ \mu_{\mathrm{P}} = \begin{cases} 0 & \text{if } de \le 0, \\ (2de) & \text{if } de \in \left(0, \frac{1}{2}\right], \\ \left(\frac{2de}{3} - \frac{4}{3}\right) & \text{if } de \in \left(\frac{1}{2}, 2\right), \\ 0 & \text{if } de \ge 2, \end{cases} \\ \mu_{\mathrm{PB}} = \begin{cases} 0 & \text{if } de \le \frac{1}{2}, \\ \left(\frac{2de}{3} - \frac{1}{3}\right) & \text{if } de \in \left(\frac{1}{2}, 2\right), \\ 1 & \text{if } de \ge 2. \end{cases} \end{cases} \tag{35}$$

The membership degrees of the fuzzy outputs U'_{ctrl1} and U'_{ctrl2} are described by the fuzzy sets C_i and D_i, which are defined by the membership functions of Figure 6.

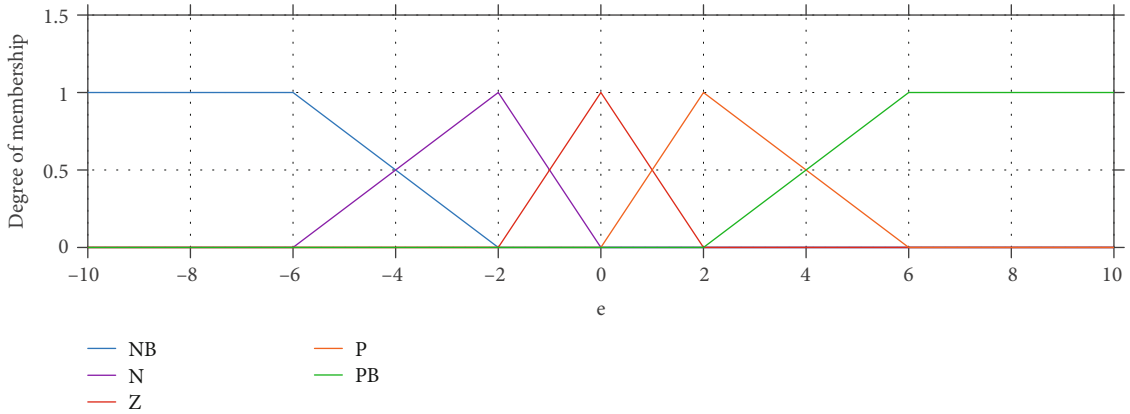

Figure 4: Membership functions for input *e*.

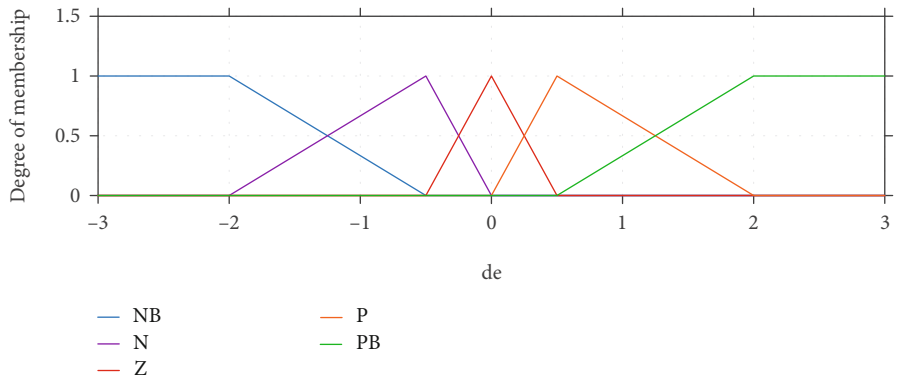

Figure 5: Membership functions for input *de*.

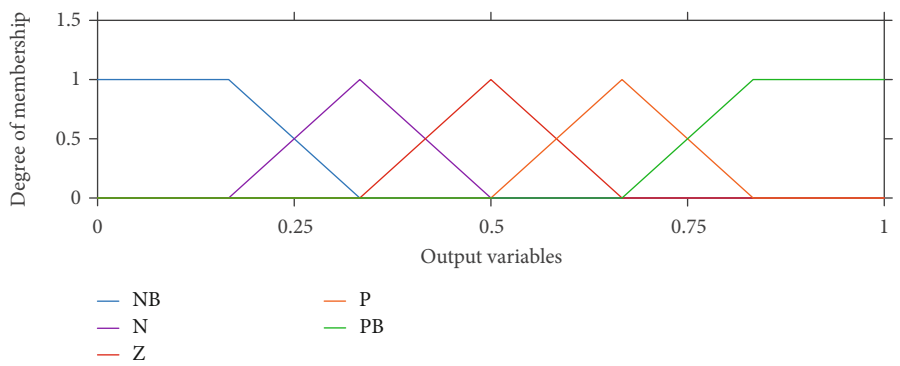

Figure 6: Membership functions for outputs U'_{ctrl1} and U'_{ctrl2}.

Therefore, the mark of the membership functions μ_{C_i} and μ_{D_i} for the fuzzy outputs U'_{ctrl1} and U'_{ctrl2} is:

$$\mu_{C_i/D_i} = \begin{cases} \mu_{\text{NB}}(X) = \begin{cases} 1 & \text{if } X \le \frac{1}{6}, \\ (-6X+2) & \text{if } X \in \left(\frac{1}{6}, \frac{1}{3}\right), \\ 0 & \text{if } X \ge \frac{1}{3}, \end{cases} \\ \mu_{\text{N}}(X) = \begin{cases} 0 & \text{if } X \le \frac{1}{6}, \\ (6X-1) & \text{if } X \in \left(\frac{1}{6}, \frac{1}{3}\right], \\ (-6X+3) & \text{if } X \in \left(\frac{1}{3}, \frac{1}{2}\right), \\ 0 & \text{if } X \ge \frac{1}{2}, \end{cases} \\ \mu_{\text{Z}}(X) = \begin{cases} 0 & \text{if } X \le \frac{1}{3}, \\ (6X-2) & \text{if } X \in \left(\frac{1}{3}, \frac{1}{2}\right], \\ (-6X+4) & \text{if } X \in \left(\frac{1}{2}, \frac{2}{3}\right), \\ 0 & \text{if } X \ge \frac{2}{3}, \end{cases} \\ \mu_{\text{P}}(X) = \begin{cases} 0 & \text{if } X \le \frac{1}{2}, \\ (6X-3) & \text{if } X \in \left(\frac{1}{2}, \frac{2}{3}\right], \\ (-6X+5) & \text{if } X \in \left(\frac{2}{3}, \frac{5}{6}\right), \\ 0 & \text{if } X \ge \frac{5}{6}, \end{cases} \\ \mu_{\text{PB}}(X) = \begin{cases} 0 & \text{if } X \le \frac{2}{3}, \\ (6X-4) & \text{if } X \in \left(\frac{2}{3}, \frac{5}{6}\right), \\ 1 & \text{if } X \ge \frac{5}{6}. \end{cases} \end{cases} \tag{36}$$

The membership functions defined for the output variables were the triangular and trapezoidal forms. The linguistic levels are negative-big (NB), negative (N), zero (Z), positive (P), and positive-big (PB).

Max-min fuzzy inference system is used; hence, the truth-value of the i_{th} rule of equation (33) is calculated as using the truth-values of antecedent clauses [59] by

$$\begin{aligned} \mu_{C_i} &= \bigcup_{U_{\text{ctrl1}} \in C_i} \left\{ \mu_{A_i}(e(t)) \cap \mu_{B_i}(de(t)) \right\}, \\ \mu_{D_i} &= \bigcup_{U_{\text{ctrl2}} \in D_i} \left\{ \mu_{A_i}(e(t)) \cap \mu_{B_i}(de(t)) \right\}, \end{aligned} \tag{37}$$

where μ_{A_i} is the degree of the membership functions for the input e and μ_{B_i} is the degree of the membership functions for the input de.

The defuzzification system used is the center of gravity technique may be defined by

$$\begin{aligned} U_{\text{ctrl1}} &= \frac{\int \mu_{C_i}\left(U'_{\text{ctrl1}}\right) U'_{\text{ctrl1}}\, dU'_{\text{ctrl1}}}{\int \mu_{C_i}\left(U'_{\text{ctrl1}}\right) dU'_{\text{ctrl1}}}, \\ U_{\text{ctrl2}} &= \frac{\int \mu_{D_i}\left(U'_{\text{ctrl2}}\right) U'_{\text{ctrl2}}\, dU'_{\text{ctrl2}}}{\int \mu_{D_i}\left(U'_{\text{ctrl2}}\right) dU'_{\text{ctrl2}}}, \end{aligned} \tag{38}$$

where μ_{C_i} is the degree of the membership functions for the output U'_{ctrl1} and μ_{D_i} is the degree of the membership functions for the output U'_{ctrl2}.

3.2. Fuzzy Rule Definition. If the platform is slanted to the front, the force resulting from the pressurized air inside the chamber of OWC1 should be superior to that of the force resulting from the pressurized air inside the chamber of OWC2. However, if the platform is slanted to the back, the force resulting from the pressurized air inside the chamber of OWC should be inferior to the force resulting from the pressurized air inside the chamber of OWC2. Hence, the control should be active for OWC1 whenever θ_p is positive to increase the pressure; however, the valve control for OWC2 should be inactive to decrease the pressure. Contrariwise, when the θ_p is negative, the valve control for OWC1 should be inactive, and the control for OWC2 should be active.

A set of 25 rules, which have been summarized in Tables 4 and 5, govern equation (33). The fuzzy rules have been selected to control the valve's opening and closing according to the platform pitch.

3.3. Fuzzy Surfaces. Using the membership functions defined in Figures 4–6, a 3D plot of the obtained fuzzy surfaces for U'_{ctrl1} is presented in Figure 7(a) and the fuzzy surfaces for U'_{ctrl2} are presented in Figure 7(b).

Based on the max-min fuzzy inference system, the crisp values of the control outputs U_{ctrl1} and U_{ctrl2} are obtained from the fuzzy outputs U'_{ctrl1} and U'_{ctrl2} using the center of gravity defuzzification technique as [58]

$$Y = Y^{\min} + \left(Y^{\max} - Y^{\min}\right) Y', \tag{39}$$

where Y is the crisp value of U_{ctrl1} and U_{ctrl2}, Y' is the fuzzy outputs U'_{ctrl1} and U'_{ctrl2} obtained from the fuzzy

Table 4: Fuzzy rules for OWC1.

U'_{ctrl1}		e				
		NB	N	Z	P	PB
de	NB	NB	N	Z	P	P
	N	NB	N	Z	P	P
	Z	NB	N	Z	P	PB
	P	N	N	Z	P	PB
	PB	N	N	Z	P	PB

Table 5: Fuzzy rules for OWC2.

U'_{ctrl2}		e				
		NB	N	Z	P	PB
de	NB	PB	P	Z	N	N
	N	PB	P	Z	N	N
	Z	PB	P	Z	N	NB
	P	P	P	Z	N	NB
	PB	P	P	Z	N	NB

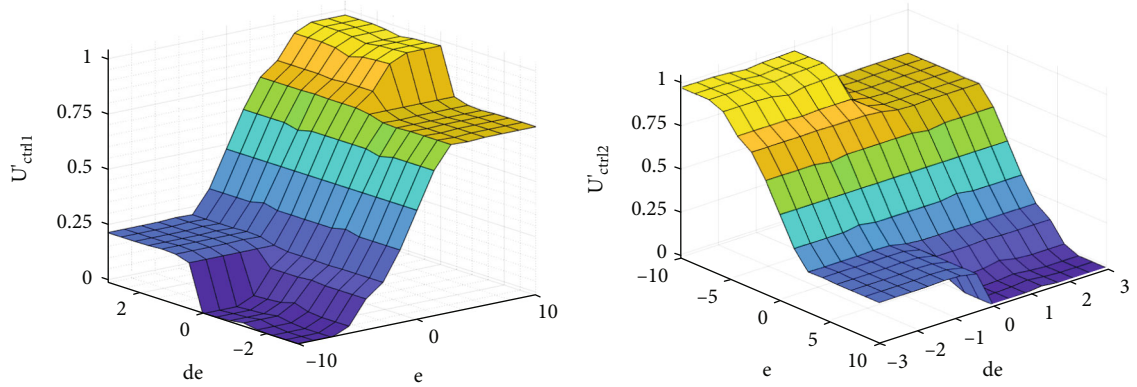

(a) Fuzzy surface for OWC1's valve

(b) Fuzzy surface for OWC2's valve

Figure 7: Fuzzy surface for OWC1 and OWC2's valves.

surfaces of Figure 7, and Y^{max} and Y^{min} are the control min and max values chosen according to the actuator.

4. Results and Discussion

This paper studies the vibration dynamics of the proposed hybrid system associated with waves. Thus, the effects of the winds on the WT were not considered in the simulations.

To assess the efficiency of the suggested fuzzy-based airflow control for the OWC-FOWT, a comparative study with a PID-based airflow control has been performed. The PID control has been developed and implemented in a previous work in [45].

4.1. Assessment and Validation Using Low-Frequency Waves. To assess the efficiency of the suggested fuzzy airflow control for the OWC-FOWT, an investigation has been performed using two regular waves with different wave periods. As illustrated in Figure 8, the considered wave input $Z(t)$ has a 1 m wave amplitude and a wave period of 30 s between 0 and 1000 s. The second half of the wave input, between 1000 and 2000 s, has a wave period of 20 s.

The simulation of the OWC-FOWT model resulted on the airflow velocity of OWC1, as shown in Figure 9, and the airflow speed of OWC2, as shown in Figure 10. The airflow of uncontrolled valves is represented by the black dotted curves, the PID controlled valves are represented by the red dashed curves, and the fuzzy controlled valves are represented by the blue solid curves.

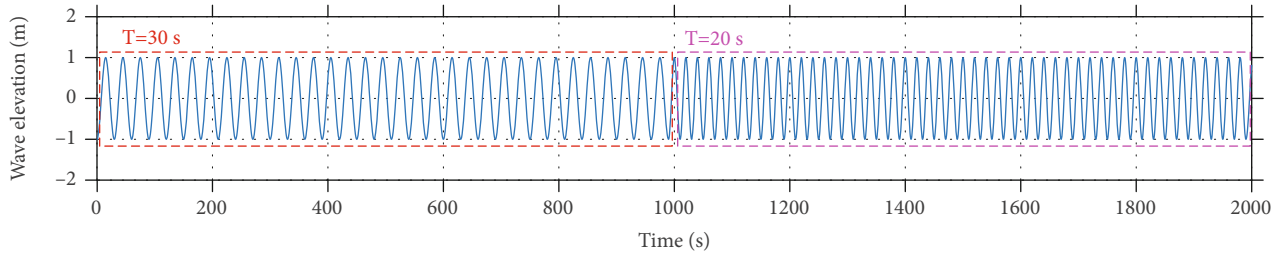

Figure 8: Introduced wave input $Z(t)$ with two wave periods.

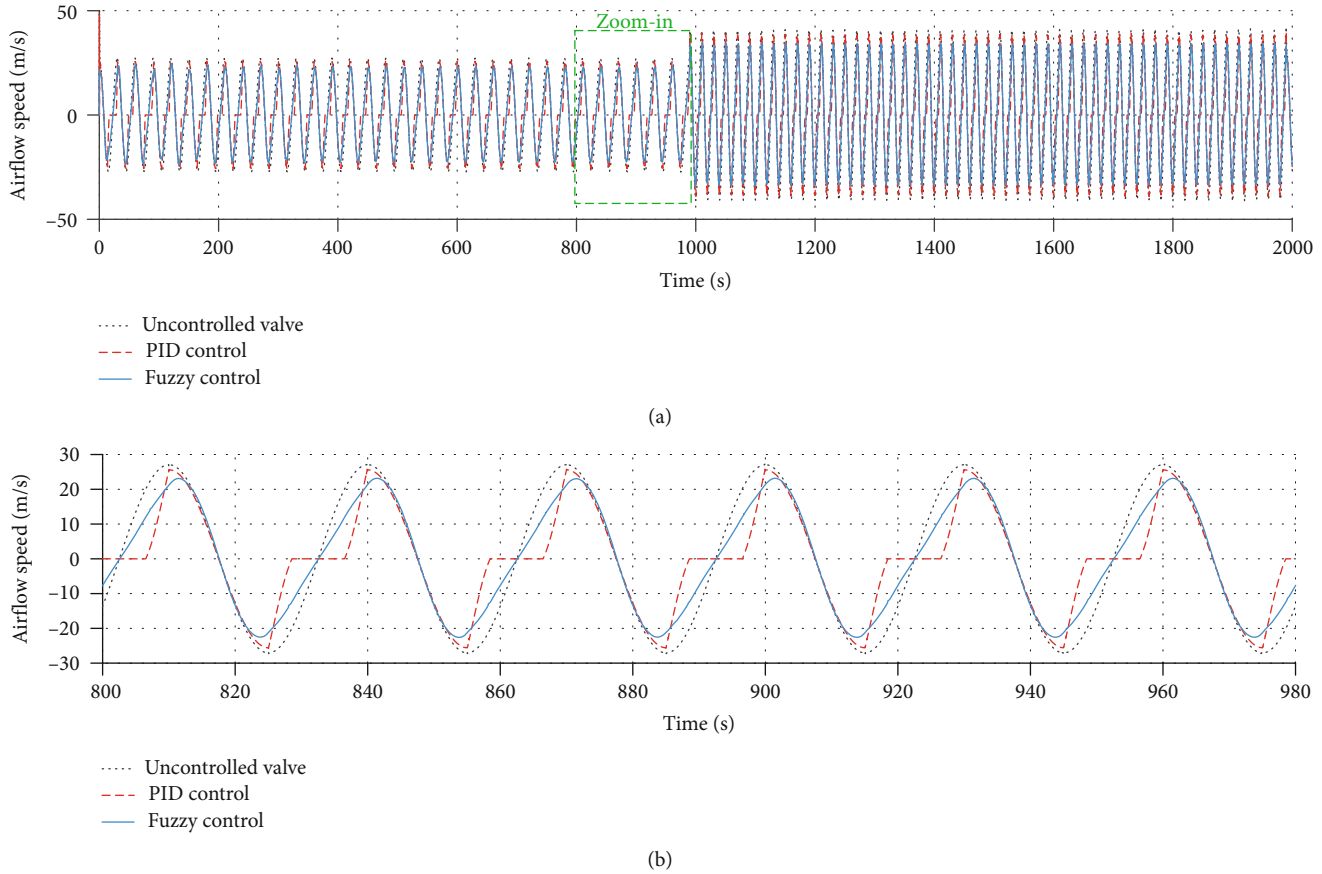

Figure 9: Obtained airflow speeds in OWC1. (a) Airflow speeds. (b) Zoom-in section.

By zooming in Figures 9(b) and 10(b), the results of utilizing the suggested airflow control may be perceived in both airflow speed of OWC1 and OWC2 in the red and blue curves, which are compared to uncontrolled valves in black curves. It can be noticed that if the control is active, the valves decrease the airflow velocity whereas the valves are always open in the black curves. However, between the PID-controlled and fuzzy-controlled valves, we can see different behaviors. It is shown that with PID controllers, the airflow is reduced to zero more abruptly whereas the fuzzy controller smoothly reduces the airflow amplitude to zero.

The subsequent pressure from the produced airflow speed of Figures 9 and 10 is presented in Figure 11 for OWC1 and in Figure 12 for OWC2 with controlled and uncontrolled valves. The results of controlled valves may be observed in the pressure in the red and blue curves. In fact, due to the valves closing, the pressure has been sustained at a superior value in comparison to the uncontrolled case (black curves) where it decreases to the atmospheric pressure value. Moreover, the pressure's average value achieved using the fuzzy control greater values than that of the pressure obtained using PID control thanks to the aforementioned smooth closing of the valves.

The achieved platform pitch of the OWC-FOWT with both PID and fuzzy controls was compared to the platform pitch of the standard FOWT in Figure 13. According to these results, the PID- and fuzzy-controlled systems manage to operate the valves according to the platform pitch and

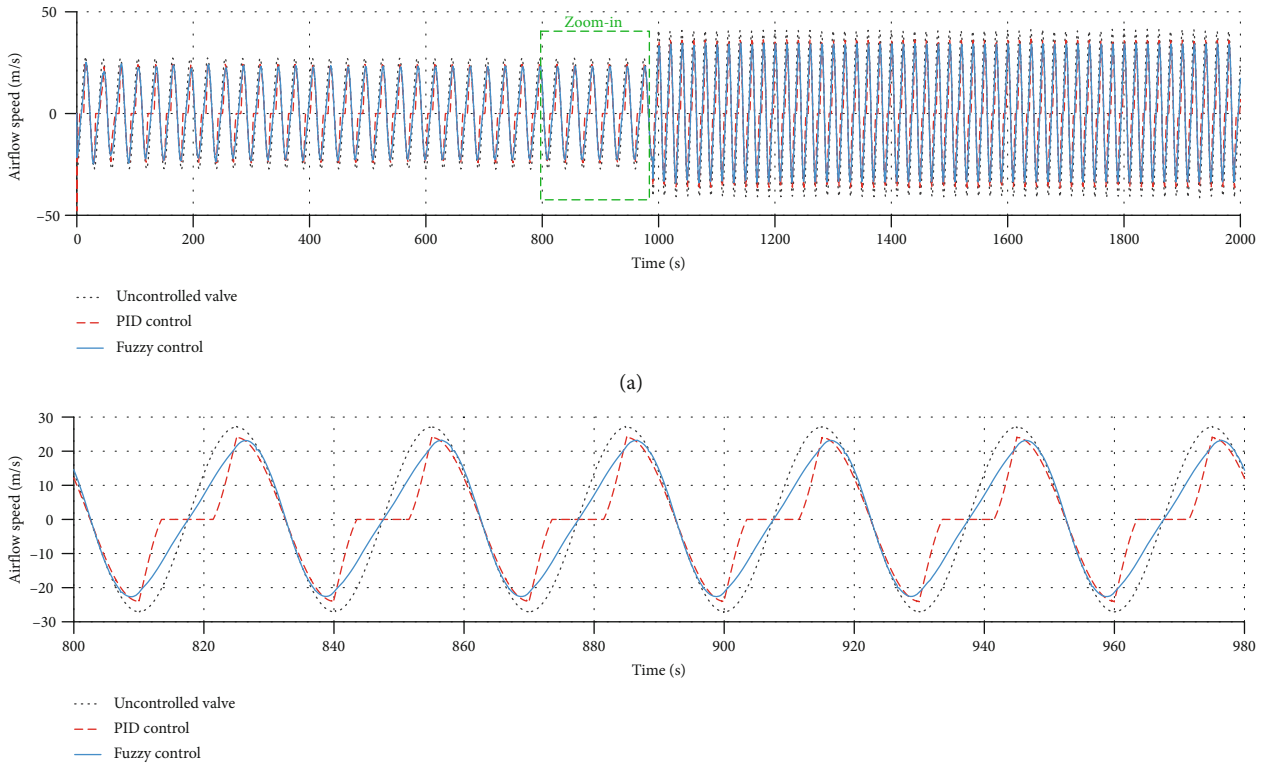

Figure 10: Obtained airflow speeds in OWC2. (a) Airflow speeds. (b) Zoom-in section.

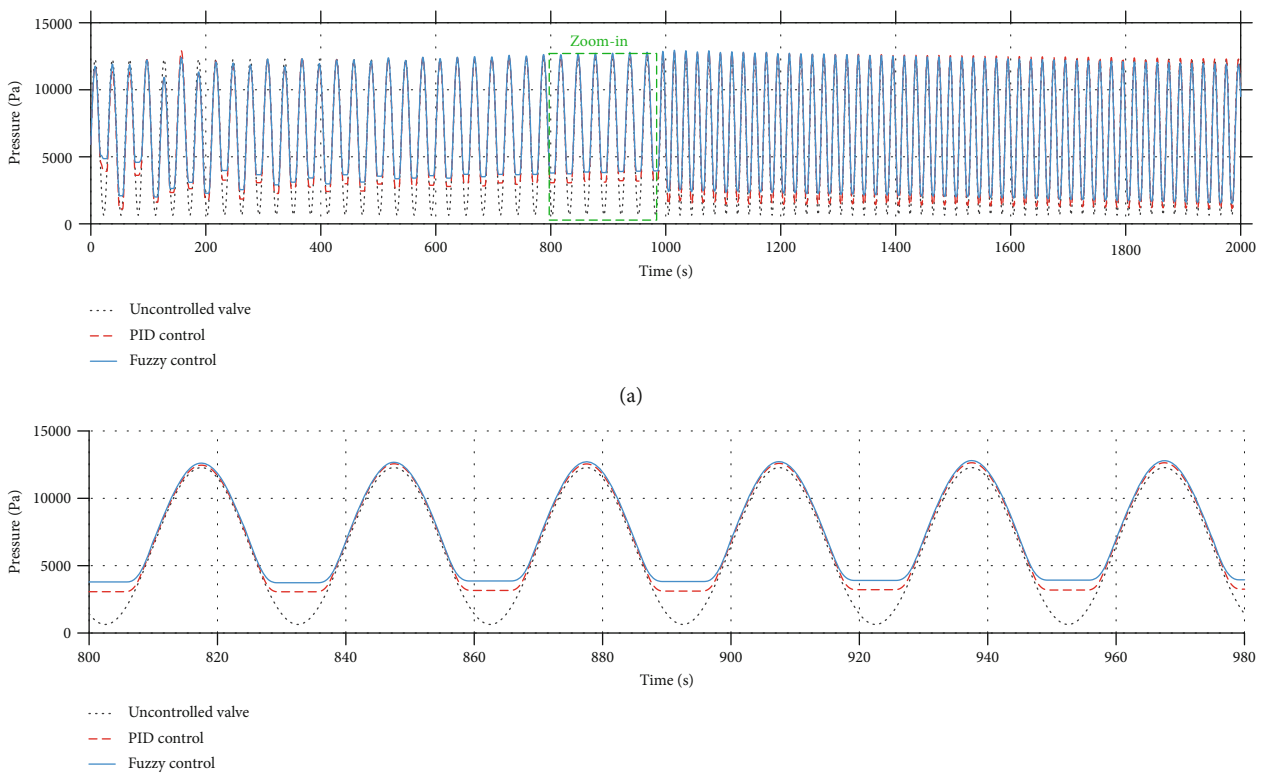

Figure 11: Obtained pressure in OWC1. (a) Chamber pressure. (b) Zoom-in section.

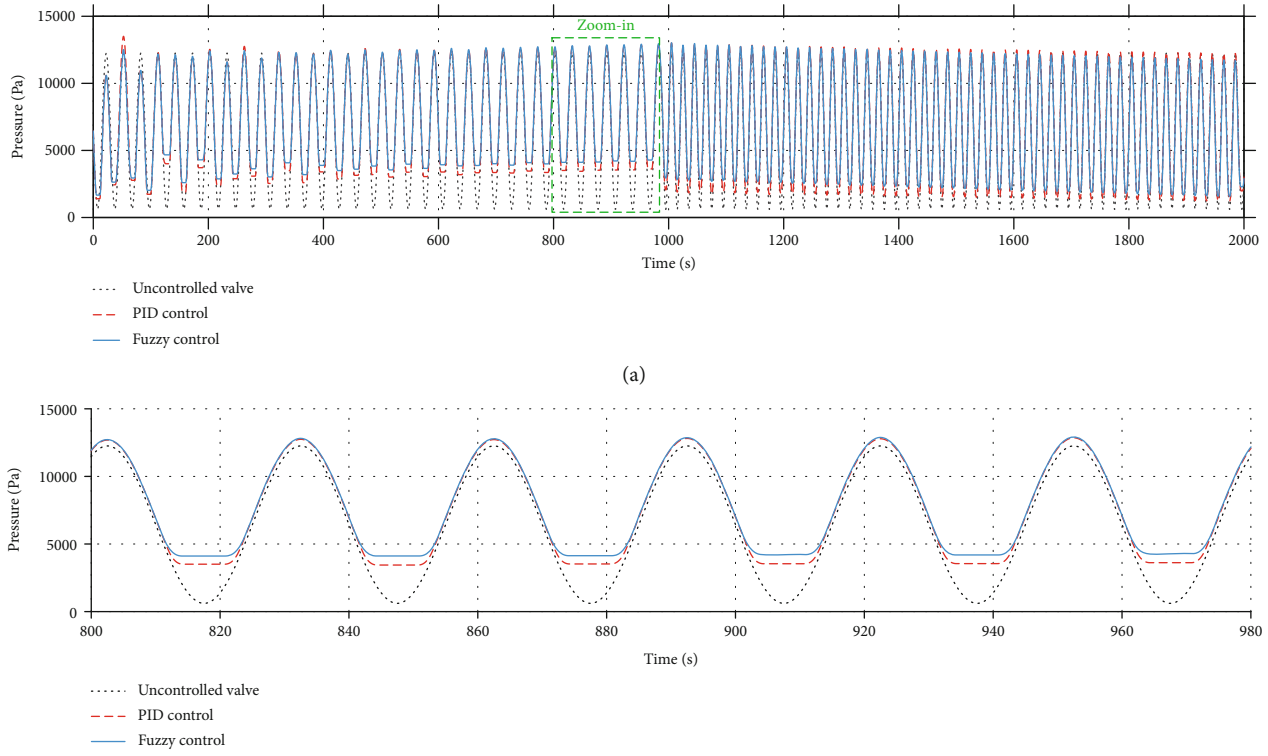

Figure 12: Obtained pressure in OWC2. (a) Chamber pressure. (b) Zoom-in section.

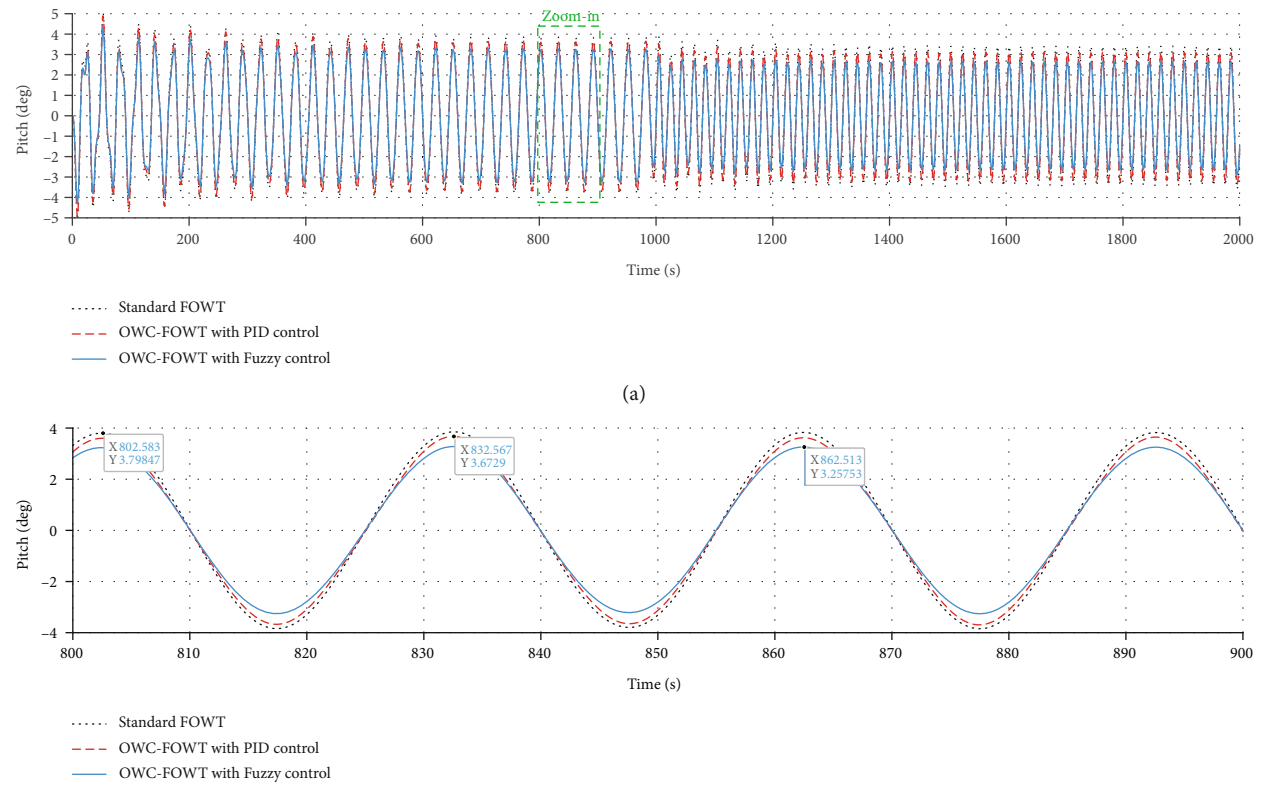

Figure 13: Obtained platform pitch. (a) Platform pitch. (b) Zoom-in section.

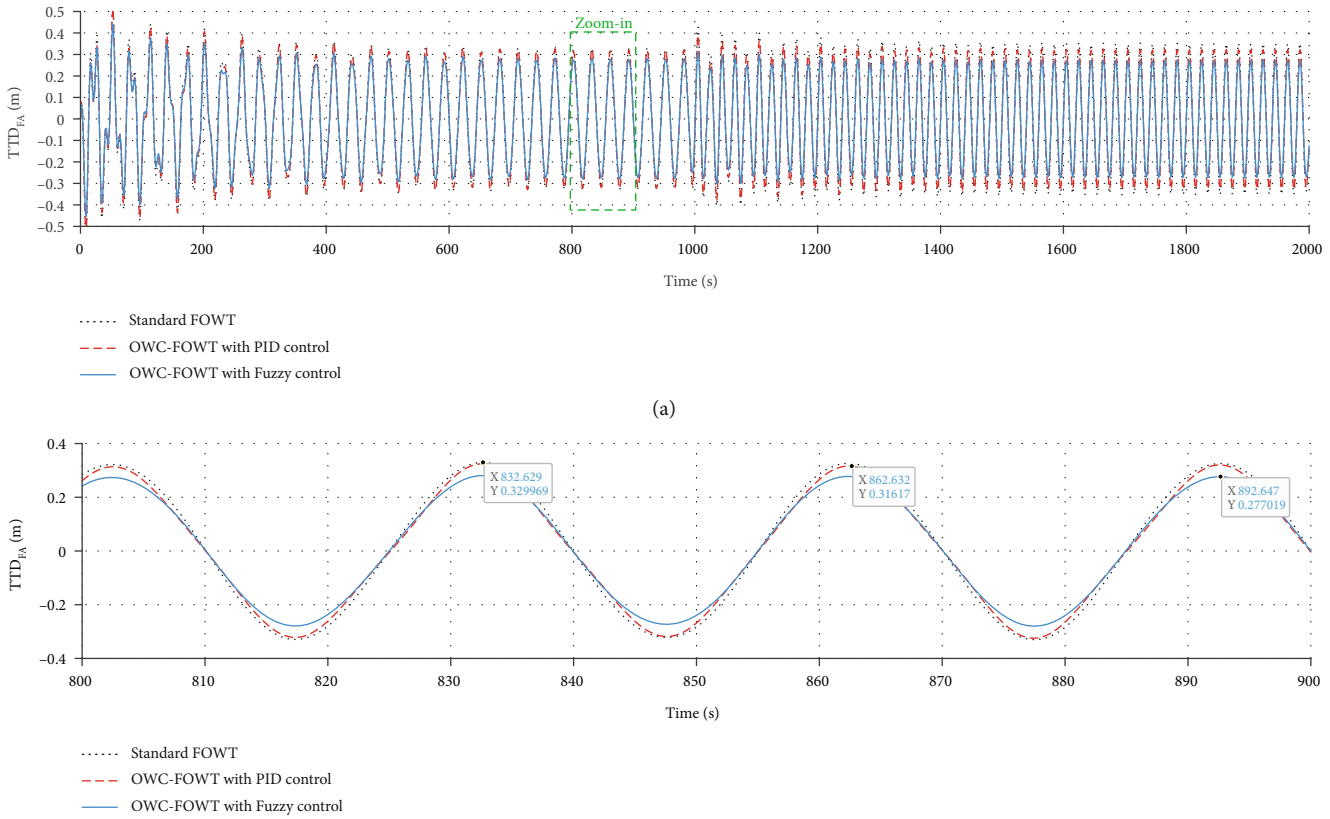

Figure 14: Obtained fore-aft tower top displacement (TTD_{FA}). (a) Fore-aft displacement. (b) Zoom-in section.

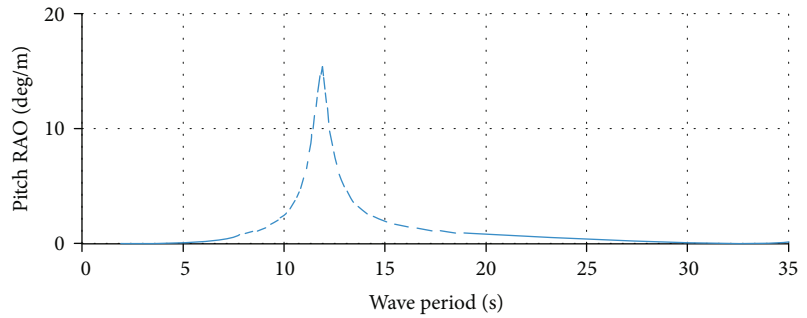

Figure 15: Pitch RAO of the floating offshore wind turbine system.

have effectively lowered the platform pitch for both wave periods. In fact, when zooming in the curves during the waves of 30 s wave period, it is observed in Figure 13(b) that the pitch angle has reduced from 3.798° in a standard barge to 3.672° in a PID-controlled OWC-based barge and to 3.257° in a fuzzy-controlled OWC-based barge. Similarly, for the 20 s period waves, the pitch has been reduced from 3.418° in a standard barge to 3.090° in a PID-controlled OWC-based barge and to 2.646° in a fuzzy-controlled OWC-based barge. The fuzzy-controlled system has further reduced the pitch thanks to the aforementioned increase in the average value of the pressure.

The simulated fore-aft tower top displacement (TTD_{FA}) of the OWC-based FOWT with both PID and fuzzy controls has been compared to the TTD_{FA} of a standard FOWT and is shown in Figure 14. Similar to the platform pitch, it is clear that the PID- and fuzzy-controlled systems have successfully reduced the TTD_{FA} during both wave conditions. Actually, when zooming into the curves during the waves of 30 s wave period, it is noticed in Figure 14(b) that the TTD_{FA} has reduced from 0.32996 m in a standard FOWT to 0.31617 m in a PID-controlled OWC-FOWT and to 0.27756 m in a fuzzy-controlled OWC-FOWT. Similarly, for the 20 s period waves, the TTD_{FA} has decreased from

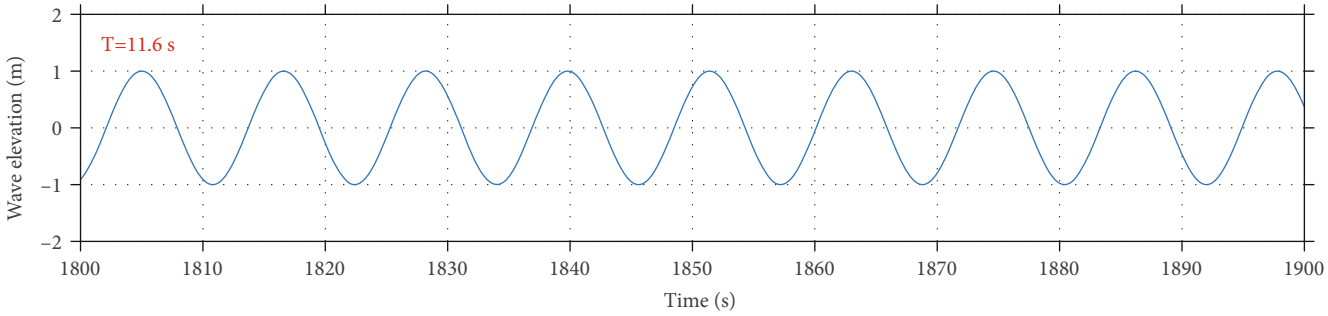

Figure 16: Introduced wave input $Z(t)$ with resonance wave period.

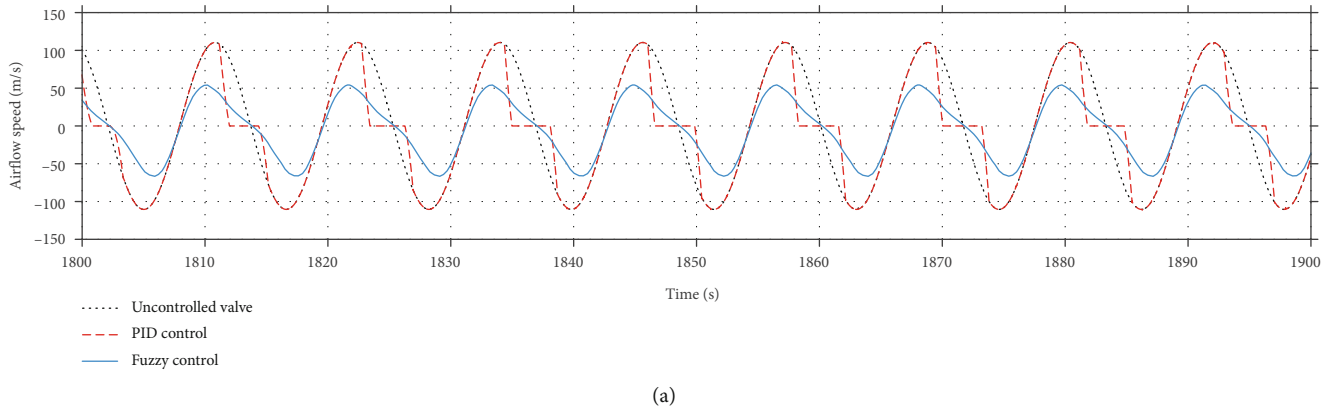

(a)

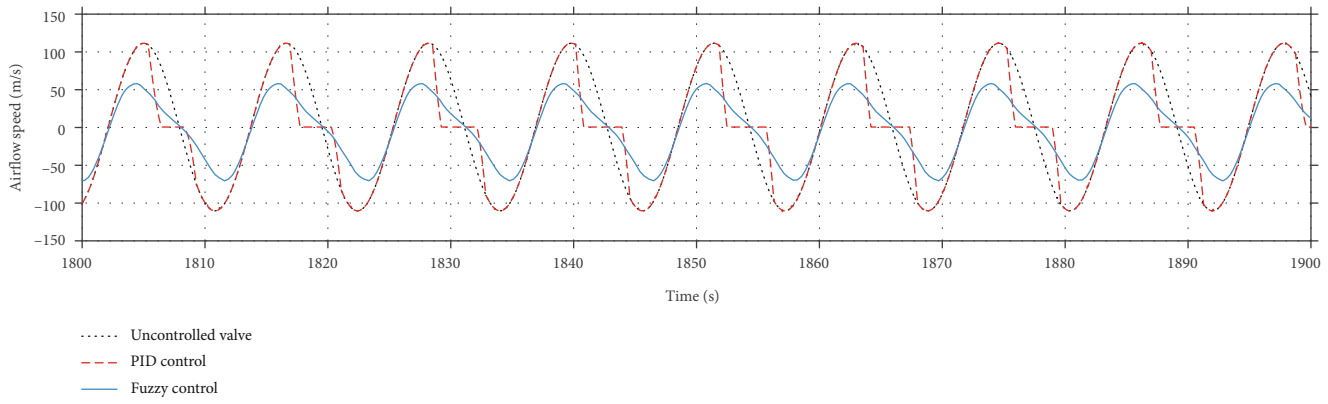

(b)

Figure 17: Obtained airflow speed (a) in OWC1 and (b) in OWC2.

0.351956 m in a standard barge to 0.321654 m in a PID-controlled OWC-based barge and to 0.272671 m in a fuzzy-controlled OWC-based barge. It is obvious that the fuzzy-controlled system has further reduced the TTD_{FA} thanks to the aforementioned increase in the average value of the pressure.

4.2. Assessment and Validation Using Resonance Frequency Waves. To further test the structural response of the proposed hybrid FOWT-OWC and to further evaluate the effectiveness of the developed fuzzy airflow control, another simulation has been carried out using the resonance frequency of the floating FOWT-OWC structure. According to the response amplitude operator (RAO) of the platform pitch illustrated in Figure 15, the resonance corresponds to waves with a period of 11.6 s.

Using the resonance wave period of Figure 15, a regular wave input of a period of 11.6 s and a wave amplitude of 1 m have been introduced to the developed model for simulation as shown in Figure 16.

The airflow obtained within the capture chambers of OWC1 and OWC2 is shown in Figures 17(a) and 17(b), in the uncontrolled case, with PID airflow control and with the fuzzy airflow control. It can be noticed that if the control is active, the valves decrease the airflow velocity whereas the valves are always open in the black curves. However,

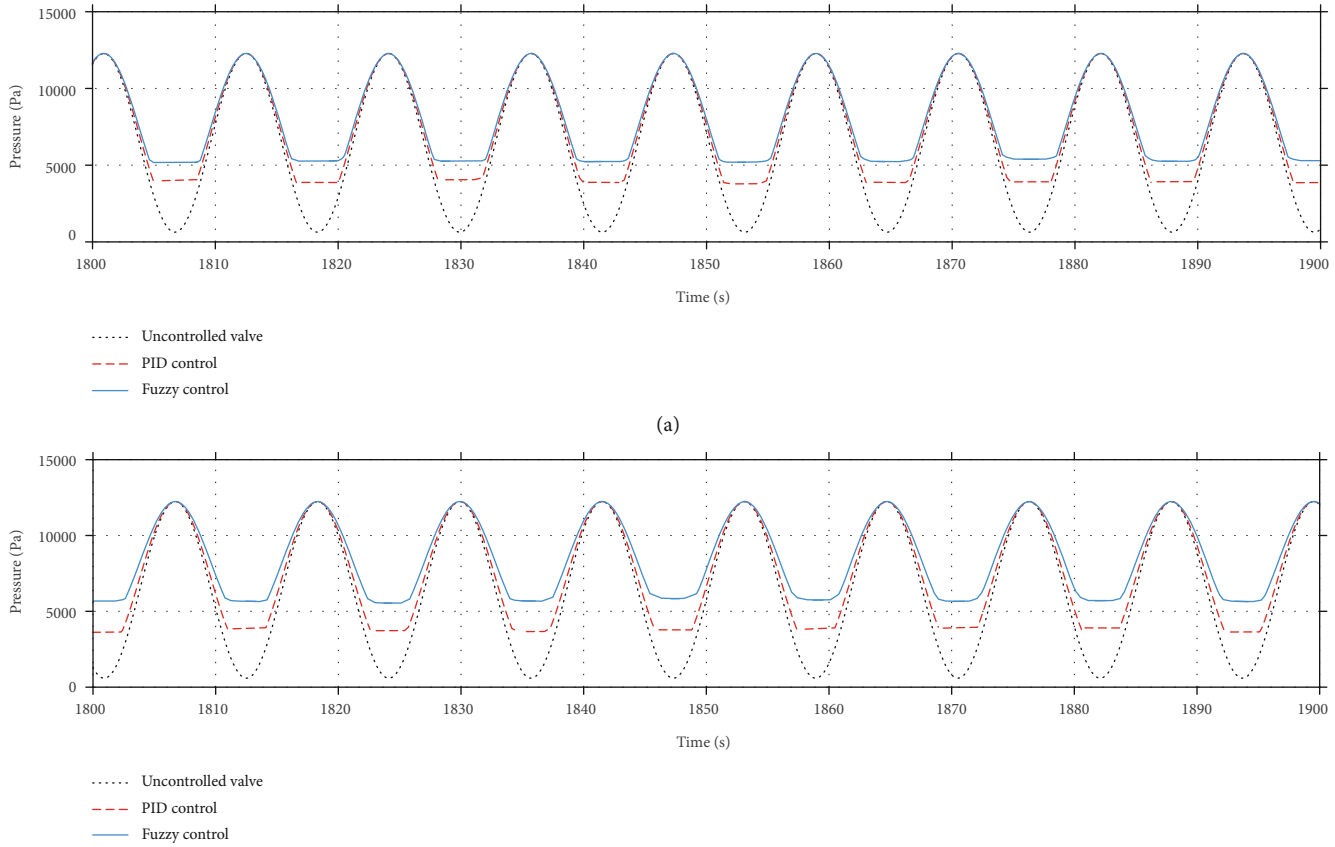

Figure 18: Obtained pressure (a) in OWC1 and (b) in OWC2.

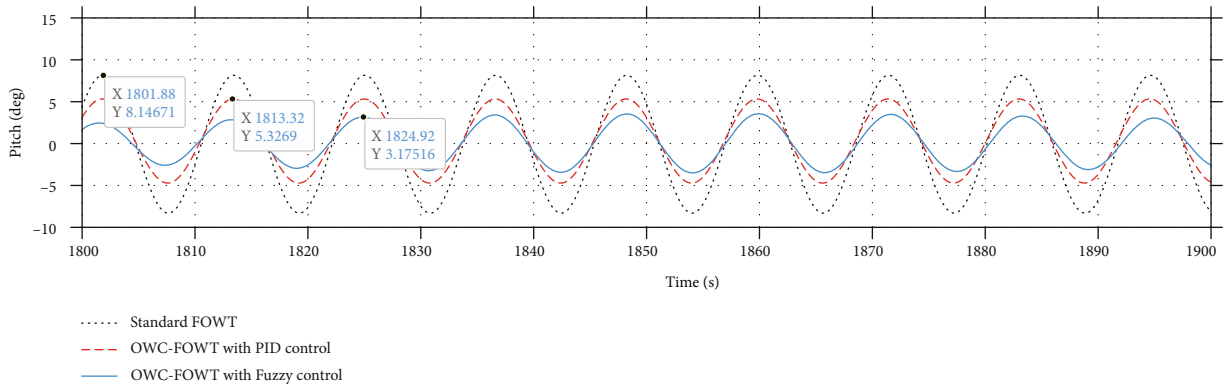

Figure 19: Obtained platform pitch for standard FOWT vs. OWC-FOWT.

between the PID-controlled and fuzzy-controlled valves, we can see different behaviors. It is shown that with PID controllers, the airflow is reduced to zero more abruptly whereas the fuzzy controller smoothly reduces the airflow amplitude to zero.

From the airflow speeds of OWC1 and OWC2 of Figure 17, the produced pressures in the capture chambers are shown in Figures 18(a) and 18(b), in the uncontrolled case, with PID airflow control and with the fuzzy airflow control. The results of the controlled valves may be observed in the pressure of the red and blue curves. In fact, due to the valves closing, the pressure has been maintained at a higher value in comparison to the uncontrolled case (black curves) where it decreases to the atmospheric pressure value. Moreover, the pressure's average value was achieved using the fuzzy control greater values than that of the pressure obtained using PID control thanks to the aforementioned smooth closing of the valves.

Consequently, the obtained platform pitch of the PID airflow-controlled OWC-FOWT and the fuzzy airflow-

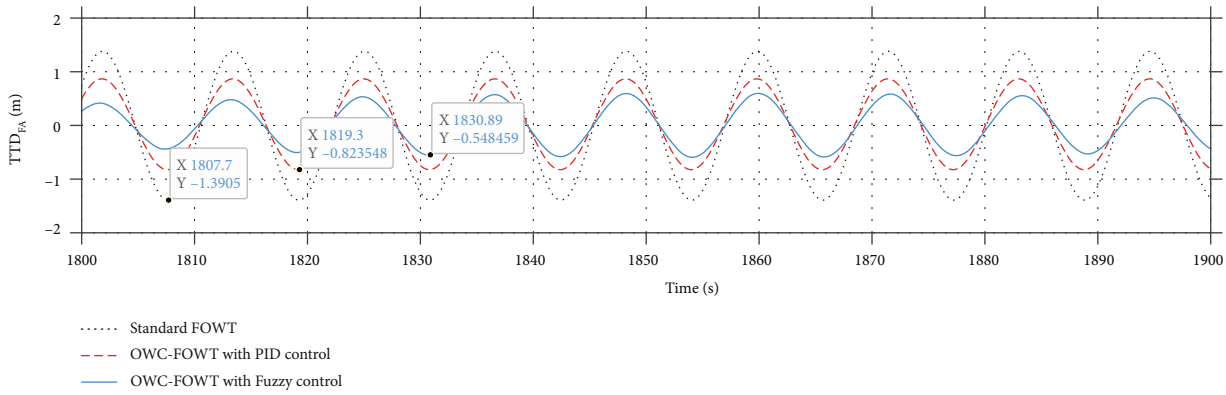

Figure 20: Obtained top tower fore-aft displacement for standard FOWT vs. OWC-FOWT.

controlled OWC-FOWT is illustrated in Figure 19 and is compared to the pitch angle of standard barge-type FOWT. According to these results, the PID and fuzzy-controlled systems manage to operate the valves according to the platform pitch and have effectively lowered the platform pitch. In fact, it is observed that the pitch angle has reduced from 8.146° in a standard barge to 5.326° in a PID-controlled OWC-based barge and to 3.175° in a fuzzy-controlled OWC-based barge. The fuzzy-controlled system has further reduced the pitch thanks to the aforementioned increase in the average value of the pressure.

The resulting fore-aft tower top displacement (TTD_{FA}) of the OWC-based FOWT with both PID and fuzzy controls has been compared to TTD_{FA} of a standard FOWT and is shown in Figure 20. Similar to the platform pitch, it is clear that the PID- and fuzzy-controlled systems have successfully reduced the TTD_{FA} during both wave conditions. Actually, the TTD_{FA} has reduced from 1.3905 m in a standard FOWT to 0.8235 m in a PID-controlled OWC-FOWT and to 0.5484 m in a fuzzy-controlled OWC-FOWT. It is obvious that the fuzzy-controlled system has further reduced the TTD_{FA} thanks to the aforementioned increase in the average value of the pressure.

As predicted from the pitch RAO of Figure 15, the platform pitch and TTD_{FA} are the highest with waves of resonance period 11.6 s. In fact, the pitch reaches 8.14°, and the TTD_{FA} reaches 1.39 m in the standard FOWT. However, similarly to the other study cases, the proposed PID-based airflow control and the fuzzy-based airflow control manage to successfully reduce the vibrations in the FOWT system.

5. Conclusions

In the presented research work, a new active structural control has been developed through the incorporation of two OWCs in an ITI Energy barge platform of a floating offshore wind turbine to attempt to stabilize the platform by reducing the platform pitch and tower top fore-aft. This concept relies on the counterforces resulting from the decompressed air inside the capture chambers to decrease the unwanted platform pitch and the tower fore-aft bending.

To do so, a dynamic simplified model of the propose hybrid OWC-based FOWT has been developed while focusing on the platform pitch and the tower top fore-aft displacement DOFs. For the developed mathematical model, the pressure and force of the OWCs have been taken into consideration in order to study the impact of integrating the OWCs to resist some of the hydrodynamic forces affecting the stability of the platform. A fuzzy airflow control for the OWCs has been implemented to gradually open and close the valves of the integrated OWCs according to the pitching of the platform. The fuzzy airflow control measures the platform pitch angle and generating fuzzy outputs to control the opening of the valves in the OWC chambers, which will adjust the pressure inside the air chambers adequately.

The results achieved show that in comparison to the standard FOWT and a PID-controlled OWC-based FOWT, with different wave periods that the proposed fuzzy-controlled OWC-based FOWT effectively decreases the vibrations of the platform pitch by an average of 14% and the tower top fore-aft bending by an average of 15%. On the other hand, the PID-controlled OWC-based FOWT decreases the vibrations of the platform pitch by an average of 3% and the tower top fore-aft bending by an average of 4%.

It is to be noted that the some of the advantages of the proposed OWC-based barge FOWT concept are that compared to the TMD and TLCD; it harvests additional energy from the waves. Also, the same control strategy can be designed to both extract maximum wave energy and stabilize the platform. However, the disadvantages are that it is a more intricate solution and that the integration of OWCs in barge platforms could be costly compared to TMD and will require new industries to reduce it.

The obtained results can be further applied to reduce other undesired oscillatory motions such as the platform roll and tower top side-to-side displacement by installing other pairs of OWCs in other directions. Also, a scaled model of a 3D printed barge platform with a small wind turbine is being tested in the 5 m wave tank of the Automatic Control Group (ACG) laboratory for experimental results.

Data Availability

No data has been used.

Conflicts of Interest

The authors declare no potential conflict of interests.

Acknowledgments

The authors would like to thank the Basque Government for funding their research work through project IT1555-22 and the Ministry of Science and Innovation (MCIN) for funding their research work through projects PID2021-123543OB-C21 and PID2021-123543OB-C22 by MCIN/AEI/10.13039/501100011033/FEDER, UE, and the University of the Basque Country (UPV/EHU) through the María Zambrano grant MAZAM22/15 funded by UPV-EHU/MIU/Next Generation, EU.

References

[1] A. Kuriqi, A. Pinheiro, A. Sordo-Ward, and L. Garrote, "Water-energy-ecosystem nexus: balancing competing interests at a run-of-river hydropower plant coupling a hydrologic-ecohydraulic approach," *Energy Conversion and Management*, vol. 223, article 113267, 2020.

[2] A. Kuriqi, A. Pinheiro, A. Sordo-Ward, and L. Garrote, "Flow regime aspects in determining environmental flows and maximising energy production at run-of-river hydropower plants," *Applied Energy*, vol. 256, article 113980, 2019.

[3] GWEC, *Global Offshore Wind Report 2020*, Tech. Rep. Technical Report, Global Wind Energy Council, Brussels, Belgium, 2020, https://gwec.net/global-offshore-wind-report-2020/.

[4] A. Darwish and R. Al-Dabbagh, "Wind energy state of the art:present and future technology advancements," *Renewable Energy and Environmental Sustainability*, vol. 5, p. 7, 2020.

[5] A. H. ZhongW, L. Shen, T. Dai, W. Fang, X. Gao, and D. Dong, "Global pattern of the international fossil fuel trade: the evolution of communities," *Energy*, vol. 123, pp. 260–270, 2017.

[6] J. Lee and F. Zhao, *GWEC Global Wind Report 2019*, Tech. Rep. Technical Report, Global Wind Energy Council, Brussels, Belgium, 2019, https://gwec.net/global-wind-report-2019/.

[7] X. Wu, Y. Hu, Y. Li et al., "Foundations of offshore wind turbines: a review," *Renewable and Sustainable Energy Reviews*, vol. 104, pp. 379–393, 2019.

[8] M. Abdel-Basset, A. Gamal, R. K. Chakrabortty, and M. Ryan, "A new hybrid multi-criteria decision-making approach for location selection of sustainable offshore wind energy stations:a case study," *Journal of Cleaner Production*, vol. 280, article 124462, 2021.

[9] D. Cevasco, S. Koukoura, and A. Kolios, "Reliability, availability, maintainability data review for the identification of trends in offshore wind energy applications," *Renewable and Sustainable Energy Reviews*, vol. 136, article 110414, 2021.

[10] GWEC, *Global Offshore Wind Report 2021*, Tech. Rep. Technical Report, Global Wind Energy Council, Brussels, Belgium, 2021, https://gwec.net/global-offshore-wind-report-2021/.

[11] G. Tomasicchio, F. D'Alessandro, A. M. Avossa et al., "Experimental modelling of the dynamic behaviour of a spar buoy-wind turbine," *Renewable Energy*, vol. 127, pp. 412–432, 2018.

[12] ASAE, "Industrialising floating offshore wind," Tech. Rep. Floating wind, Equinor A.S.A, Stavanger, Norway, 2021, https://www.equinor.com/energy/floating-wind.

[13] Floating OffshoreWind Farmsch, *Floating OffshoreWind Platforms*, Springer, Cham, 2016.

[14] J. Mas-Soler, E. Uzunoglu, G. Bulian, and A. Soares, "An experimental study on transporting a free-float capable tension leg platform for a 10 MW wind turbine in waves," *Renewable Energy*, vol. 179, pp. 2158–2173, 2021.

[15] R. Pool, "Deepwater wind turbines," *Engineering & Technology*, vol. 5, no. 3, p. 46, 2010.

[16] Q. Dong, J. Yang, and X. Guo, "Measurements of current loads on side-by-side semi-submersibles in a wind tunnel," *Ocean Engineering*, vol. 201, article 107126, 2020.

[17] D. Roddier, C. Cermelli, A. Aubault, and A. Weinstein, "Wind-float: a floating foundation for offshore wind turbines," *Journal of Renewable and Sustainable Energy*, vol. 2, no. 3, article 033104, 2010.

[18] A. Coulling, A. Goupee, A. Robertson, J. Jonkman, and H. Dagher, "Validation of a FAST semi-submersible floating wind turbine numerical model with DeepCwind test data," *Journal of Renewable and Sustainable Energy*, vol. 5, no. 2, article 023116, 2013.

[19] J. Jonkman and M. L. Buhl Jr., "Loads analysis of a floating offshore wind turbine using fully coupled simulation," in Tech. Rep. No. NREL/CP-500-41714, National Renewable Energy Lab. (NREL), Golden, CO, USA, 2007, https://www.nrel.gov/docs/fy07osti/41714.pdf.

[20] F. Beyer, T. Choisnet, M. Kretschmer, and P. Cheng, "Coupled MBS-CFD simulation of the IDEOL floating offshore wind turbine foundation compared to wave tank model test data," in *The Twenty-fifth International Ocean and Polar Engineering Conference*, pp. 367–374, Kona, Hawaii, USA, 2015.

[21] T. Chuang, W. Yang, and R. Yang, "Experimental and numerical study of a barge-type FOWT platform under wind and wave load," *Ocean Engineering*, vol. 230, article 109015, 2021.

[22] A. Robertson and J. Jonkman, "Loads analysis of several offshore floating wind turbine concepts," in *21st International Offshore and Polar Engineering Conference (ISOPE)*, pp. 443–450, Maui, Hawaii, USA, 2011.

[23] J. Jonkman, *Dynamics modeling and loads analysis of an offshore floating wind turbine*, Tech. Rep. No. NREL/TP-500-41958, National Renewable Energy Lab.(NREL), Golden, CO, USA, 2007, https://www.nrel.gov/docs/fy08osti/41958.pdf.

[24] J. Jonkman and D. Matha, *Quantitative comparison of the responses of three floating platforms*, Tech. Rep. No. NREL/CP-500-46726, National Renewable Energy Lab. (NREL), Golden, CO, USA, 2010, https://www.nrel.gov/docs/fy10osti/46726.pdf.

[25] M. Lackner, "Controlling platform motions and reducing blade loads for floating wind turbines," *Wind Engineering*, vol. 33, no. 6, pp. 541–553, 2009.

[26] A. Staino and B. Basu, "Emerging trends in vibration control of wind turbines: a focus on a dual control strategy," *Philosophical Transactions of the Royal Society A: Mathematical, Physical and Engineering Sciences*, vol. 373, no. 2035, article 20140069, 2015.

[27] J. Yang, Y. He, Y. Zhao, X. Yang, and G. Zhang, "Coupled dynamic response analysis of multi-column floating offshore wind turbine with low center of gravity," *Journal of Ocean Engineering and Science*, pp. 1–15, 2022.

[28] K. Cheung, A. Phadke, D. Smith, S. Lee, and L. Seidl, "Hydrodynamic response of a pneumatic floating platform," *Ocean Engineering*, vol. 27, no. 12, pp. 1407–1440, 2000.

[29] M. Lackner and M. Rotea, "Passive structural control of offshore wind turbines," *Wind Energy*, vol. 14, no. 3, pp. 373–388, 2011.

[30] N. Luo, L. Pacheco, Y. Vidal Seguí, and H. Li, "Smart structural control strategies for offshore wind power generation with floating wind turbines," *Renewable Energies & Power Quality Journal*, vol. 1, pp. 1200–1205, 2012.

[31] Y. Hu and E. He, "Active structural control of a floating wind turbine with a stroke-limited hybrid mass damper," *Journal of Sound and Vibration*, vol. 410, pp. 447–472, 2017.

[32] J. Hu, B. Zhou, C. Vogel et al., "Optimal design and performance analysis of a hybrid system combing a floating wind platform and wave energy converters," *Applied Energy*, vol. 269, article 114998, 2020.

[33] J. Sarmiento, A. Iturrioz, V. Ayllón, R. Guanche, and I. Losada, "Experimental modelling of a multi-use floating platform for wave and wind energy harvesting," *Ocean Engineering*, vol. 173, pp. 761–773, 2019.

[34] J. Yu, Z. Li, Y. Yu et al., "Design and performance assessment of multi-use offshore tension leg platform equipped with an embedded wave energy converter system," *Energies*, vol. 13, no. 15, p. 3991, 2020.

[35] Z. Gao, T. Moan, L. Wan, and C. Michailides, "Comparative numerical and experimental study of two combined wind and wave energy concepts," *Journal of Ocean Engineering and Science*, vol. 1, no. 1, pp. 36–51, 2016.

[36] J. Kluger, A. Slocum, and T. Sapsis, "A first-order dynamics and cost comparison of wave energy converters combined with floatingwind turbines," in *The 27th International Ocean and Polar Engineering Conference*, pp. 577–585, San Francisco, CA, USA, 2017.

[37] Z. Ma, W. Li, N. Ren, and J. Ou, "The typhoon effect on the aerodynamic performance of a floating offshore wind turbine," *Journal of Ocean Engineering and Science*, vol. 2, no. 4, pp. 279–287, 2017.

[38] A. Slocum, J. Kluger, and S. Mannai, "Energy harvesting and storage system stabilized offshore wind turbines," in *2019 Offshore Energy and Storage Summit (OSES)*, Brest, France, 2019.

[39] M. Kamarlouei, J. Gaspar, M. Calvario et al., "Experimental analysis of wave energy converters concentrically attached on a floating offshore platform," *Renewable Energy*, vol. 152, pp. 1171–1185, 2020.

[40] M. Khatibani and M. Ketabdari, "Numerical modeling of an innovative hybrid wind turbine and WEC systems performance: a case study in the Persian Gulf," *Journal of Ocean Engineering and Science*, pp. 1–16, 2022.

[41] Z. Zhu and H. Changhong, "A study on control of wave energy converter for motion suppression of semisubmersible," *IFAC-PapersOnLine*, vol. 49, no. 23, pp. 380–385, 2016.

[42] J. Sierra-García and M. Santos, "Redes neuronales y aprendizaje por refuerzo en el control de turbinas eólicas," *Revista Iberoamericana de Automática e Informática industrial*, vol. 18, no. 4, pp. 327–335, 2021.

[43] X. Li and G. Huijun, "Load mitigation for a floating wind turbine via generalized H_∞ structural control," *IEEE Transactions on Industrial Electronics*, vol. 63, pp. 332–342, 2016.

[44] F. Yang, Q. Song, Q. Wang, S. Zuo, and S. Li, "Wind and wave disturbances compensation to floating offshore wind turbine using improved individual pitch control based on fuzzy control strategy," *IEEE Transactions on Industrial Electronics*, vol. 2014, article 968384, pp. 1–10, 2014.

[45] F. M'zoughi, P. Aboutalebi, I. Garrido, A. Garrido, and M. De La Sen, "Complementary airflow control of oscillating water columns for floating offshore wind turbine stabilization," *Mathematics*, vol. 9, no. 12, article 1364, 2021.

[46] P. Aboutalebi, F. M'zoughi, I. Garrido, and A. Garrido, "Performance analysis on the use of oscillating water column in barge-based floating offshore wind turbines," *Mathematics*, vol. 9, no. 5, p. 475, 2021.

[47] F. M'zoughi, I. Garrido, S. Bouallégue, M. Ayadi, and A. Garrido, "Intelligent airflow controls for a stalling-free operation of an oscillating water column-based wave power generation plant," *Electronics*, vol. 8, no. 1, p. 70, 2019.

[48] F. M'zoughi, I. Garrido, A. Garrido, and M. De La Sen, "ANN-based airflow control for an oscillating water column using surface elevation measurements," *Sensors*, vol. 20, no. 5, p. 1352, 2020.

[49] F. M'zoughi, I. Garrido, A. Garrido, and M. De La Sen, "Selfadaptive global-best harmony search algorithm-based airflow control of a wells-turbine-based oscillating-water column," *Applied Sciences*, vol. 10, no. 13, p. 4628, 2020.

[50] W. Vijfhuizen, *Design of a Wind and Wave Power Barge, [M.S. thesis]*, Department of Naval Architecture and Mechanical Engineering, Universities of Glasgow and Strathclyde, 2006.

[51] J. Jonkman, "Influence of control on the pitch damping of a floating wind turbine," in *46th AIAA aerospace sciences meeting and exhibit*, pp. 1–15, Reno, Nevada, USA, 2008.

[52] G. Stewart and M. Lackner, "Offshore wind turbine load reduction employing optimal passive tuned mass damping systems," *IEEE Transactions on Control Systems Technology*, vol. 21, no. 4, pp. 1090–1104, 2013.

[53] M. Lackner and M. Rotea, "Structural control of floating wind turbines," *Mechatronics*, vol. 21, no. 4, pp. 704–719, 2011.

[54] C. Perez-Collazo, D. Greaves, and G. Iglesias, "A review of combined wave and offshore wind energy," *Renewable and Sustainable Energy Reviews*, vol. 42, pp. 141–153, 2015.

[55] A. Aubault, M. Alves, A. Sarmento, D. Roddier, and A. Peiffer, "Modeling of an oscillating water column on the floating foundation WindFloat," in *30th International Conference on Ocean, Offshore & Arctic Engineering (OMAE 2011)*, pp. 235–246, Rotterdam, the Netherlands, 2011.

[56] Y. Hu, J. Wang, M. Z. Chen, Z. Li, and Y. Sun, "Load mitigation for a barge-type floating offshore wind turbine via inerter-based passive structural control," *Engineering Structures*, vol. 177, pp. 198–209, 2018.

[57] E. He, Y. Hu, and Y. Zhang, "Optimization design of tuned mass damper for vibration suppression of a barge-type offshore floating wind turbine," *Proceedings of the Institution of Mechanical Engineers, Part M: Journal of Engineering for the Maritime Environment*, vol. 231, no. 1, pp. 302–315, 2017.

[58] Z. Zhao, M. Tomizuka, and S. Isaka, "Fuzzy gain scheduling of PID controllers," *IEEE Transactions on Systems, Man, and Cybernetics*, vol. 23, no. 5, pp. 1392–1398, 1993.

[59] C. Lee, "Fuzzy logic in control systems: fuzzy logic controller. I," *IEEE Transactions on Systems, Man, and Cybernetics*, vol. 20, no. 2, pp. 404–418, 1990.

[60] J. Zhao and B. Bose, "Evaluation of membership functions for fuzzy logic controlled induction motor drive," in *IEEE 2002 28th Annual Conference of the Industrial Electronics Society. IECON 02*, pp. 229–234, Sevilla; Spain, 2002.

[61] A. Sadollah, *Fuzzy logic based in optimization methods and control systems and its applicationsch. Introductory Chapter: Which Membership Function is Appropriate in Fuzzy System?*, IntechOpen, 2018.